Early arc development recorded in Permian–Triassic plutons of the northern Mojave Desert region, California, USA

M. Robinson Cecil[1,†], Mary Ann Ferrer[1], Nancy R. Riggs[2], Kathleen Marsaglia[1], Andrew Kylander-Clark[3], Mihai N. Ducea[4,5], and Paul Stone[6]

[1]*Department of Geological Sciences, California State University–Northridge, Northridge, California 91130, USA*
[2]*School of Earth Sciences and Environmental Sustainability, Northern Arizona University, Flagstaff, Arizona 86011, USA*
[3]*Department of Earth Science, University of California at Santa Barbara, Santa Barbara, California 93106, USA*
[4]*Department of Geosciences, University of Arizona, Tucson, Arizona 85721, USA*
[5]*Faculty of Geology and Geophysics, University of Bucharest, Bucharest, Romania 010041*
[6]*U.S. Geological Survey, Menlo Park, California 94025, USA*

ABSTRACT

Permian–Middle Triassic plutons in the northern Mojave Desert, USA, are emplaced into the cryptic El Paso terrane, which is characterized by a northwest-striking belt of deep marine eugeoclinal strata juxtaposed against Proterozoic basement and its miogeoclinal cover. Fourteen new zircon U-Pb ages from the El Paso Mountains and Lane Mountain region of the Mojave Desert record nearly continuous magmatism occurring between ca. 275 and 240 Ma. These ages, which are taken to record the onset of subduction-related magmatism along the southwestern Laurentian margin, are older than the earliest arc plutons documented in the southern Sierra Nevada region to the north and in the Transverse Ranges to the south. They overlap, however, with Permian arc plutons documented in Sonora, Mexico. Dated plutons are compositionally variable, but can be characterized as intermediate to felsic, calcic to calc-alkalic, and having chemistries consistent with generation in an arc setting. Whole rock Sr-Nd isotopic compositions vary widely from relatively primitive ($Sr_i = 0.7035$, initial $\varepsilon Nd = +3$, initial εHf in zircon = +13) to moderately evolved ($Sr_i = 0.708$, initial $\varepsilon Nd = -5$, initial εHf in zircon = –3). Isotopic signatures differ considerably from partially coeval Triassic suites of the Transverse Ranges and central Mojave, which are more evolved and consistent with emplacement in Proterozoic continental crust of the Mojave province. They also differ considerably from those typical of intermediate plutons generated in intra-oceanic arcs, which are overall much more mantle-like. This suggests that the underpinnings of the El Paso terrane may be at least partly composed of continental crust and that magmas emplaced into the terrane may have been variably contaminated by crustal components. This is supported by the presence of Precambrian and early Paleozoic zircon inheritance recorded in some plutons. In all isotopic systems, values are the most evolved in the oldest plutons (ca. 275–270 Ma), becoming more juvenile in the Middle Triassic. These temporal trends, together with pluton fabrics and new estimates of Permian plate vectors, are interpreted to reflect generation of the earliest arc in a contractional setting that may have driven crustal thickening and a greater involvement of crustal materials in Permian magmas. This result supports a model of forced subduction initiation, which is favored by a change in plate motions along a previously weak margin, and predicts an initial compressive state in the upper plate. The uniformly primitive signatures of Triassic melts are taken to indicate a change to a transtensional upper-plate stress regime that promoted the development of more voluminous, primarily mantle-derived melts. Regional pluton age patterns suggest that arc magmatism initiated in restricted areas of the southwestern Laurentian margin (northern Mojave, Sonora) and then migrated north and south ultimately becoming a continuous arc by Jurassic time.

INTRODUCTION

Andean-type magmatic arcs record the growth-scales and modification of continental crust. The generation and reworking of continental crust at convergent margins is one of the key tenets of plate tectonics, yet the initiation of subduction and the generation of the earliest arc magmatic products are not commonly studied. This is likely due, at least in part, to poor preservation of early arc magmas in many arcs, especially in continental settings. The first magmas produced, following the inception of subduction, may shed light on stress conditions in the upper plate and help constrain models for mode of subduction initiation (e.g., spontaneous versus forced; Hall et al., 2003; Gurnis et al., 2004; Stern, 2004; Leng and Gurnis, 2011). It is therefore of critical importance to identify and study rocks that represent such magmas wherever they occur.

The SW Cordilleran margin of North America underwent significant tectonic change in the Paleozoic, ultimately transitioning from a passive margin in the mid-Paleozoic to a subduction zone by the Triassic. Proterozoic to mid-Paleozoic SW-trending passive margin facies belts, which track across Nevada and eastern California, USA, are truncated along a NW-oriented trend that roughly parallels the prominent Mesozoic batholithic belts (e.g., Sierra Nevada and Peninsular Ranges batholiths) (e.g., Burchfiel and Davis, 1972; Stone and Stevens, 1988; Walker, 1988; Dickinson and Lawton, 2001; Stevens et al., 2005). That truncation likely resulted from the development of a NW-SE sinistral strike-slip system (California-Coahuila transform of Dickinson

†robinson.cecil@csun.edu

and Lawton, 2001) that tectonically reshuffled crustal fragments along the margin prior to the initiation of subduction. Permian–Middle Triassic intrusions of the Mojave region are uniquely positioned, both temporally and spatially, to record this tectonically complex passive margin to subduction system transition.

The Cordilleran magmatic arc of California was produced by nearly continuous subduction beneath the western continental margin of North America from late Paleozoic to late Mesozoic time. Although this arc has been extensively studied, relatively little is known about its oldest plutons, most of which have been obliterated by younger magmatic activity. This contribution uses new geochronologic, geochemical, and isotopic data from a suite of late Paleozoic plutons uniquely preserved in the central Mojave Desert region, to investigate the initial stages of arc development and to broaden our understanding of how a magmatic arc first develops in a nascent subduction zone. We build on earlier geochronologic work by reporting new single-grain zircon U-Pb ages for the earliest arc plutons that were previously difficult to accurately date via bulk zircon methods due to Pb loss, inheritance, or a combination of the two (Miller et al., 1995; Carr et al., 1997). Geochronology, together with new geochemical and isotopic characteristics of the plutons, are used to constrain: (1) the timing of subduction initiation in the SW Cordillera, (2) the petro-tectonic conditions of early continental arc growth, (3) the paleogeographic limits and the timing of displacement of parautochthonous blocks, across which the early arc is emplaced, and (4) the mode of subduction initiation in the late Paleozoic Cordilleran margin.

REGIONAL GEOLOGIC AND TECTONIC SETTING

Arc magmatism in the southwestern USA was active throughout the Mesozoic, generating a NNW-striking belt of largely intermediate intrusive rocks that today form the backbone of the Cordillera in the region. Magmatism occurred in three documented pulses in Late Triassic, Middle Jurassic, and Cretaceous times, the last of which was the most voluminous, producing most of the plutons that make up the large and spatially distinct Sierra Nevada and Peninsular Ranges batholiths (e.g., Ducea, 2001; DeCelles et al., 2009; Barth et al., 2013; Premo et al., 2014; Paterson et al., 2011; Paterson and Ducea, 2015). Between those two batholiths lies a tectonically complex segment of the Cordilleran margin where subduction-related intrusive rocks are disaggregated, cropping out in the Transverse Ranges of southern California (Barth et al., 1997, 2008) and in isolated ranges

across the Mojave Desert region (Miller and Morton, 1980; Beckerman et al., 1982; Miller and Sutter, 1982; Schermer and Busby, 1994; Miller and Glazner, 1995; Miller et al., 1995). Although most of the batholithic exposures in these areas are similarly dominated by Cretaceous intrusions, smaller, arc-related plutons in the central Mojave and nearby regions are late Permian to Middle Triassic in age (Miller et al., 1995; Barth et al., 1997; Barth and Wooden, 2006; Saleeby and Dunne, 2015) (Fig. 1). These intrusions are of interest both because of their age and because of their unique position within the tectonic framework of the southwestern Cordilleran margin.

The Mojave Block

The Mojave block is a wedge-shaped region of southern California that is tectonically
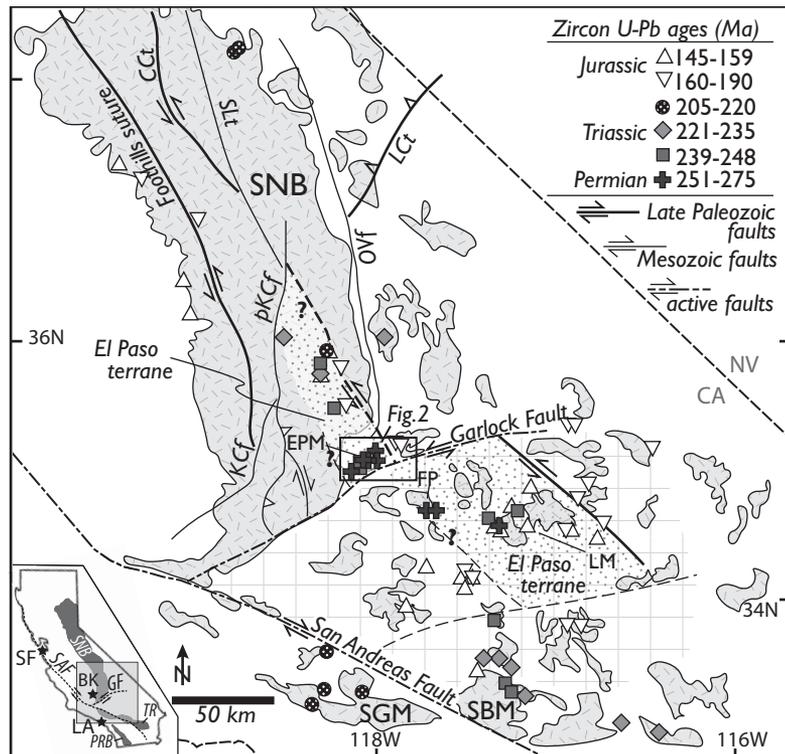
Figure 1. Generalized tectonic map of south-central California, USA, showing the distribution of dated Permian and Triassic plutons. Mesozoic batholithic rocks of the Sierra Nevada, Mojave Desert, and Transverse Ranges are shown in the gray patterned regions. Pale yellow region represents proposed extent of the El Paso terrane (see text for discussion). Mesozoic faults are shown as heavy red lines and major late Paleozoic faults are shown as heavy black lines. CCt—California Coahuila transform; EPM—El Paso Mountains; FP—Fremont Peak; KCf—Kern Canyon fault; LM—Lane Mountain; LCt—Last Chance thrust; OVf—Owens Valley fault; pKCf—proto-Kern Canyon fault; SBM—San Bernardino Mountains; SGM—San Gabriel Mountains; SLt—Snow Lake transform. Data sources for pluton ages are from: this study, Miller et al. (1995); Barth et al. (1997, 2011); Barth and Wooden (2006); and Saleeby and Dunne (2015). Map is modified after Chapman et al. (2015). Inset map: Gray box represents the map area. Blue stars are cities in California, USA: BK—Bakersfield; LA—Los Angeles; SF—San Francisco. Dark gray polygons are the approximate areas of batholithic segments discussed in the text: PRB—Peninsular Ranges batholith; SNB—Sierra Nevada batholith; TR—central and eastern Transverse Ranges. Modern faults are shown as red dashed lines: GF—Garlock fault; SAF—San Andreas Fault.

bounded by the sinistral Garlock fault to the north, the Big Bend segment of the dextral San Andreas Fault system to the west and south, and the southern extension of the Death Valley shear zone to the east (Glazner et al., 2002) (Fig. 1). This Mojave block and adjacent regions (the southwesternmost Great Basin to the north and the eastern Transverse Ranges to the south) occupy a unique position within the Cordilleran tectonic framework because they link the northern and southern segments of the Basin and Range province, connect the modern transform boundary with inboard deformation that accommodates some of the Pacific-North American plate motion, and separate the Sierra Nevada batholith from batholithic segments exposed in the Transverse Ranges and Peninsular Ranges to the south.

The pre-Cenozoic geology of the Mojave Desert region is dominated by Mesozoic plutonic and volcanic rocks, which resulted from the growth of the Cordilleran continental arc above a long-lived subduction zone (e.g., Dickinson, 2004). The basement to the Mesozoic arc includes Cambrian–early Permian nearshore (miogeoclinal) strata and deeper-water off-shelf (eugeoclinal) passive-margin deposits (Burchfiel and Davis, 1972, 1975; Stewart and Poole, 1975; Miller and Sutter, 1982; Carr et

al., 1984; Walker, 1988; Martin and Walker, 1992, 1995). Exposures of Precambrian basement are rare in this part of the Mojave, though they are commonly found in the eastern Mojave Desert (Wooden and Miller, 1990; Coleman et al., 2002; Wooden et al., 2013) and the Transverse Ranges to the south (Barth et al., 2000, 2001). Coeval with, and subsequent to development of the Cordilleran arc in the area, the Mojave and southern Sierra Nevada regions experienced tectonic disruption, including extension, metamorphic core complex development, and rotation of fault blocks, which has led to the dismemberment of Mesozoic batholithic fragments throughout the block (e.g., Glazner et al., 1989; Dokka, 1989; Walker et al., 1990; Martin et al., 1993; Chapman et al., 2012). The majority of exposed magmatic rocks are Late Cretaceous in age, though Jurassic magmatism is also well-represented across the Mojave (e.g., Schermer and Busby, 1994; Miller and Glazner, 1995; Gerber et al., 1995; Barth et al., 2017). Middle to Late Triassic plutons are also present in restricted locations along the southern margin of the Mojave block in the eastern Transverse Ranges (Barth et al., 1997; Barth and Wooden, 2006) (Fig. 1). Permian–Middle Triassic intrusive rocks are much less common, and where exposed, are usually deformed

and/or intruded by later magmas (Miller et al., 1995; Barth and Wooden, 2006; Saleeby and Dunne, 2015).

El Paso Mountains Geology and the El Paso Terrane

The El Paso Mountains (EPM) are an eastnortheast–trending uplift located immediately north of the Garlock fault (Figs. 1 and 2). Although not part of the modern tectonic setting of the Mojave block, we group the EPM together with the central-northern Mojave because together they constitute a NW-trending belt of early arc magmatic products. The western EPM are composed of variably deformed and compositionally heterogeneous Permian–Triassic plutons. The eastern EPM are composed of the Early Jurassic Laurel Mountain pluton, which is cut by numerous Late Jurassic dikes presumably related to the Independence dike swarm. Bookended by these intrusive suites, the central EPM are composed of a structurally complex section of Paleozoic (Cambrian through Permian) strata that has undergone greenschist facies metamorphism. These strata represent a diverse assemblage of marine clastic rocks dominated by slate and meta-argillite interbedded with altered mafic volcanics, chert, and minor calcarenites
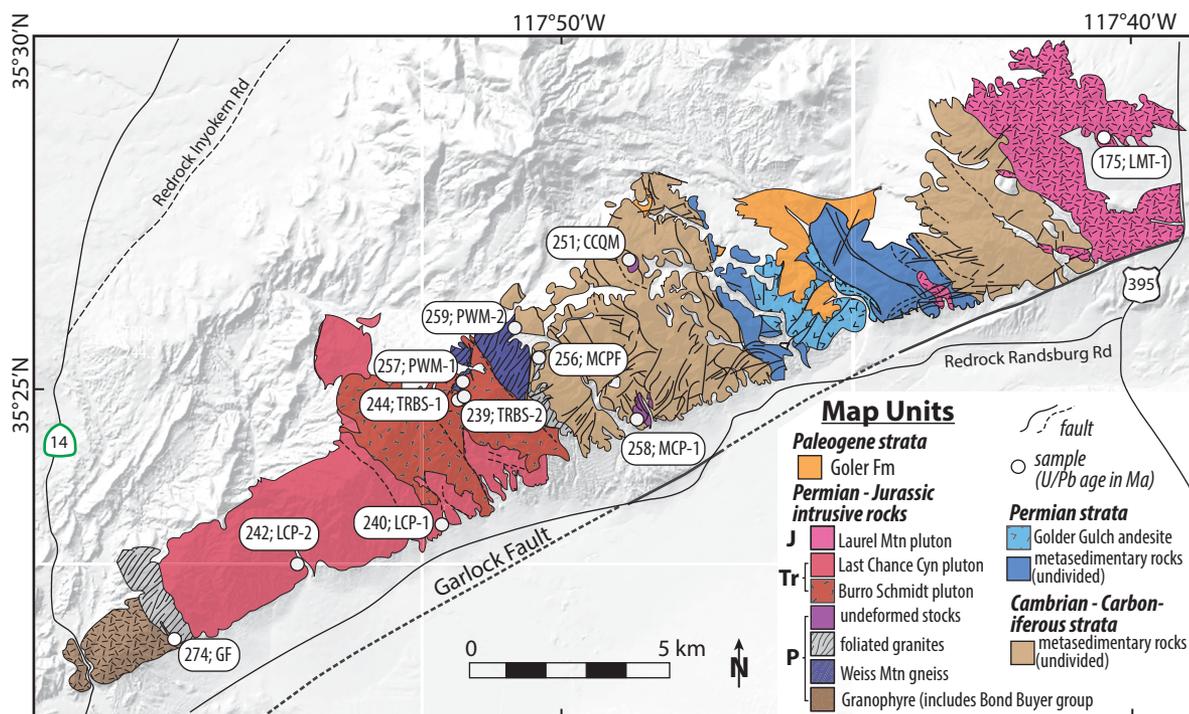
Figure 2. Geologic map of the El Paso Mountains, south-central California, USA, showing locations and approximate zircon U/Pb ages of sampled plutons. Geology modified after Christiansen (1961), Carr et al. (1997), and Dibblee and Minch (2008).

and limestones (Christiansen, 1961; Dibblee, 1967; Carr et al., 1992, 1997). The base of the Permian section is marked by metaconglomerates that grade upward into fine-grained slates and meta-argillites. These are overlain by arkosic meta-sandstones and volcanic-pebble conglomerates that are in turn conformably capped by Permian (ca. 260 Ma) andesites (Martin and Walker, 1995). This Permian sequence has been interpreted to reflect dynamic deepening and shallowing associated with the initiation of subduction in the region, which ultimately led to the emergence of arc volcanism in the late Permian (Rains et al., 2012).

Paleozoic strata similar to the metasedimentary rocks described above are also found in isolated outcrops in the central and northern Mojave (Miller and Sutter, 1982; Carr et al., 1992) and in pendants of the Kern plateau, southeastern Sierra Nevada (Dunne and Suczek, 1991). These Paleozoic packages of deep marine "eugeoclinal" rocks together make up a NW-trending belt of pendants termed the El Paso terrane (Saleeby and Dunne, 2015). Interpreted to have formed in a deep-water (off-shelf) setting, they are distinct from coeval strata exposed to the east, which are dominated by shallow-marine shelf facies. The lithologies and interpreted depositional setting of El Paso terrane strata, together with their tectonic juxtaposition against near-shore facies, has led to their correlation with similar strata of the Roberts Mountain allochthon (Poole and Sandberg, 1977; Carr et al., 1981, 1984; Burchfiel and Davis, 1981). This is further supported by similarities in detrital zircon spectra between Paleozoic pendants of the El Paso terrane in the Kern plateau region (Saleeby and Dunne, 2015) and the northwestern Mojave/Tehachapi Mountains region (Chapman et al., 2012) and coeval strata of the Roberts Mountain allochthon (Smith and Gehrels, 1994; Gehrels et al., 2000). The most recent view regarding Roberts Mountain-affinity rocks in the southern California region posits that fragments of the allochthonous terrane were translated hundreds of kilometers southward along a sinistral continental truncation fault (Stevens and Stone, 1988; Stone and Stevens, 1988; Walker, 1988; Dickinson, 2000; Stevens et al., 2005). As Saleeby and Dunne (2015) point out, however, no mid-Paleozoic (Antler-aged) deformation has been identified nor have any exposures of the Antler lower plate (outer-shelf strata) been found in the El Paso terrane. Permian–Middle Triassic early arc plutons (discussed in detail in subsequent sections) all likely intrude the El Paso terrane and can therefore provide important information about: (1) the timing of purported truncation, translation, and subduction initiation, and (2) the type of lithosphere that underlies El Paso terrane strata.

Previously Published Ages for Permian–Triassic Plutons of the El Paso Mountains and Central Mojave Regions

The Permian–Triassic plutons investigated as part of this study are all intermediate to felsic intrusive rocks exposed in ranges of the north-central Mojave (Lane Mountain and Fremont Peak areas) and north of the Mojave block along the Garlock fault (Fig. 1). We consider these rocks to represent the earliest development of the California arc system. Previously reported ages for some of these plutons (given in Table 1) include hornblende K-Ar ages of 239 Ma and 238 Ma for the Last Chance Canyon and Burro Schmidt plutons, respectively (Cox and Morton, 1980). These K-Ar dates may be minimum ages given the propensity of the system to be reset by later magmatism. Carr et al. (1997) present ages of 249 Ma (zircon U-Pb) and 252 Ma (hornblende Ar-Ar) for the Weiss Mountain gneiss and a zircon U-Pb lower intercept age of 242 Ma for the foliated granitic pluton in Mesquite Canyon (re-dated herein as MCPF). The Last Chance Canyon pluton and Weiss Mountain gneiss were subsequently dated via multi-grain thermal ionization mass spectrometry (TIMS) (Miller et al., 1995) in order to more accurately date the timing of early arc development in the area. Crystallization ages presented in Miller et al. (1995) for the Last Chance Canyon pluton and the Weiss Mountain gneiss are older (246 Ma and 260 Ma, respectively), though these are upper intercept ages defined by discordia arrays (Table 1). Miller et al. (1995) also dated a diorite body in the Lane Mountain region and an orthogneiss near Fremont Peak (Fig. 1). The diorite yielded concordant fractions with an age of 240 Ma (re-dated herein as LM-1), while the Fremont Peak orthogneiss (re-dated herein as FPG-1) yielded discordant fractions that did not define a discordia array.

ANALYTICAL METHODS

Samples were collected from nearly all mapped intrusive bodies in the EPM in order to characterize the timing and nature of early arc magmatism in the area. Samples were also collected from a foliated granodiorite in the Fremont Peak region and from two plutons in the Lane Mountain region. These were chosen because previous zircon geochronology by multi-grain TIMS from similar lithologies in the area yielded discordant Permian–Triassic ages (Miller et al., 1995). Rocks were cleaned of any weathering rinds and disaggregated using standard crushing and pulverizing techniques. A small aliquot of each pulverized sample was then powdered in an alumina ceramic shatter-

box and retained for bulk rock geochemistry and Sr-Nd isotopic analysis. The remaining sample was processed to concentrate zircon using standard density separation techniques. A magnetic separation was performed using a Frantz isodynamic separator to isolate the least magnetic zircon fraction. Zircon separates were further purified using a stereo zoom microscope. Approximately 50 individual crystals from each sample were selected based on their clarity and morphology and were mounted, together with zircon standards, in ~2.5 cm epoxy discs. Those discs were then polished to a 3 μm finish and imaged using both backscattered electron and cathodoluminescence (CL) detectors on an FEI Quanta scanning electron microscope at California State University, Northridge, USA.

Zircon U-Pb ages and Hf isotope ratios were determined using laser ablation–inductively coupled plasma–mass spectrometry (LA-ICP-MS) at the University of California, Santa Barbara, USA. Zircons ablation was performed using an Analyte G2 (Photon Machines) 193 nm ArF laser ablation system and a spot size of 25 μm. Uranium, Pb, and Hf isotopic ratio measurements were made using a Nu Instruments multicollector ICP-MS (see Kylander-Clark et al., 2013 for details of analytical methods). Using CL images as a guide, 15–30 spots per sample were chosen for U-Pb age determinations. Analytical uncertainties for reported $^{238}U/^{206}Pb$ ages are ~1 to 2% (2σ) and include both systematic and analytical errors. Following U-Pb analysis, Hf isotope ratios were obtained for each dated zircon by ablating a ~40 μm spot on top of, or adjacent to, the U-Pb ablation pit. Sample information, U-Pb ages and average Hf isotope values are summarized in Table 1. All isotope data for every zircon analysis is given in the Data Repository file[1].

Major and trace element geochemistry was performed on powdered aliquots of each sample by Actlabs (Ontario, Canada). Sample powders were fused using a lithium metaborate flux, diluted, and analyzed by quadrupole ICP-MS. Geochemical data are summarized in Table 2. Rb-Sr and Sm-Nd isotopic analysis of whole rock powders was performed at the University of Arizona, Tucson, Arizona, USA, via isotope dilution TIMS, using both an automated VG Sector multicollector instrument with adjustable 10^{11} Ω Faraday collectors and a Daly photomultiplier (Otamendi et al., 2009) and a VG Sector 54 instrument (Appendix; Drew et al.,

---

TABLE 1. SAMPLE INFORMATION, WEIGHTED MEAN AGES AND Hf ISOTOPE VALUES

Sample	Latitude (°N)	Longitude (°W)	Rock type	Foliated?	$^{206}Pb/^{238}U$ age (Ma)*	Previous age (Ma)	$\varepsilon Hf_{(t)}$[†]
El Paso Mountains							
CCQM-1	35.44723	–117.94674	Qtz Monzonite	N	251.1 ± 3.3		2.2 ± 0.6
MCPF	35.42497	–117.94674	Granodiorite	Y	255.8 ± 3.3	242[a]	1.7 ± 1.9
GF	35.35682	–117.94674	Granite	Y	273.7 ± 4.4		–0.7 ± 1.0
PWM-1	35.35682	–117.86275	Qtz Mnzdiorite	Y	257.2 ± 3.3	249[a], 256[b]	6.1 ± 0.7
PWM-2	35.43068	–117.84965	Qtz Mnzdiorite	Y	258.8 ± 3.3		n.d.
TRBS-1	35.41405	–117.86480	Hbl Qtz Diorite	N	244.3 ± 3.1		9.5 ± 0.6
TRBS-2	35.41492	–117.86418	Granite	N	238.6 ± 3.2		10.3 ± 0.6
MCP-1	35.40982	–117.81410	Tonalite	N	258.3 ± 3.5		9.6 ± 0.7
LCP-1	35.38472	–117.86965	Tonalite	N	239.5 ± 3.0	245[b]	9.3 ± 0.6
LCP-2	35.38472	–117.85184	Granodiorite	N	241.7 ± 3.4		10.0 ± 0.6
LMT-1	35.47210	–117.67361	Qtz Mnzdiorite	N	176.1 ± 2.4	170[b]	–8.1 ± 0.6
Fremont Peak							
FPG-1	35.17856	–117.47048	Granodiorite	Y	269.7 ± 3.5	260[b]	2.1 ± 0.7
Lane Mountain							
LM-1	35.09492	–117.06655	Qtz Diorite	N	252.6 ± 4.3	240[b]	5.7 ± 1.8
LM-4	35.09845	–117.04656	Qtz Monzonite	N	148.9 ± 2.3		2.7 ± 1.9

Notes: Previously published ages are all zircon U-Pb ages. Data sources are: a—Carr et al. (1997); b—Miller et al. (1995). *n.d.*—no data; Qtz Monzonite—quartz monzonite; Qtz Mnzdiorite—quartz monzodiorite; Qtz Diorite—quartz diorite; Hbl Qtz Diorite—hornblende quartz diorite. All samples are from southern California, USA.
*Errors are 2σ and include systematic and analytical uncertainties.
[†]Weighted mean; errors are 2σ.

TABLE 2. MAJOR AND TRACE ELEMENT GEOCHEMISTRY

Sample:	CCQM-1	MCPF	GF	PWM-1	PWM-2	TRBS-1	TRBS-2	MCP-1	LCP-1	LCP-2	LMT-1	FPG-1	LM-1	LM-4
SiO_2	60.31	64.38	75.48	63.83	65.04	58.28	75.72	63.89	61.1	72.15	64.24	63.04	62.43	68.41
TiO_2	0.694	0.425	0.203	0.391	0.427	0.839	0.087	0.472	0.539	0.269	0.605	0.586	0.251	0.405
Al_2O_3	18.2	17.11	13.77	16.52	16.31	15.89	13.51	15.21	17.52	14.63	15.6	17.17	19.57	16.14
MgO	1.58	1.65	0.26	1.45	1.55	2.71	0.18	2.14	1.89	0.64	2.16	2.1	0.94	1.22
FeO^{*}	4.74	3.54	1.66	4.86	3.84	6.02	1.37	6.85	5.21	2.30	5.43	5.15	3.09	3.25
MnO	0.149	0.165	0.016	0.155	0.096	0.192	0.028	0.135	0.162	0.107	0.082	0.135	0.131	0.079
CaO	5.14	3.76	1.55	5.32	4.72	6.15	1.2	4.91	5.28	2.72	4.16	5.51	6.03	3.97
K_2O	2.74	1.93	2.52	1.8	2.92	3.51	4.74	1.51	1.98	3.61	3.65	1.84	1.49	2.17
Na_2O	4.07	3.29	4.21	3.72	3.42	2.32	3.12	3.32	4.04	3.28	2.96	1.84	5.08	3.6
P_2O5	0.29	0.14	0.04	0.14	0.16	0.26	0.03	0.18	0.2	0.2	0.2	0.21	0.17	0.15
Total	100.3	100.4	100.7	99.45	100.2	99.85	100.6	100.7	100.2	100.6	100.6	100.6	100.1	100.6
A/CNK	0.96	1.19	1.10	0.93	0.94	0.85	1.08	0.95	0.95	1.02	0.95	0.98	0.93	1.04
Ba	1093	1230	1118	1229	1280	1241	729	856	706	1784	826	869	721	855
Sr	1072	374	174	569	583	404	212	634	580	409	383	509	854	511
Y	27	19	23	18	19	24	12	15	20	17	31	22	13	17
Zr	171	133	142	133	125	131	42	125	152	100	178	140	93	144
Ga	23	19	14	18	16	17	13	19	19	15	18	18	21	17
Rb	72	176	90	43	67	125	112	35	58	85	148	59	44	71
Nb	13	9	8	10	12	11	6	8	7	10	13	10	5	11
Cs	b.l.d.	10.5	1.4	1.4	2	6.7	3.5	b.l.d.	1.8	2.9	4.3	0.6	0.5	1.9
La	44.6	22.1	23.7	28.2	24	21.9	9.4	18.6	16.9	25.2	43.5	17	19.8	24.6
Ce	82.8	40.5	43.6	49.9	49.2	45.7	15.2	37.7	32.7	44.5	85.6	37	32.2	46.5
Pr	9.27	4.46	4.35	5.14	5.67	5.65	1.35	4.38	3.81	4.46	9.43	4.66	3.57	5.16
Nd	34	16	14.6	18.3	21.1	22.4	4.3	16.8	15.7	15.1	33.7	19	12.8	18.4
Sm	7.1	3.3	2.8	3.5	3.9	4.9	0.7	3.3	3.4	2.5	6.4	4.3	2.4	3.5
Eu	1.87	0.95	064	0.98	1.06	1.12	0.25	0.94	1.02	0.73	1.24	1.23	0.81	0.89
Gd	5.8	2.9	2.8	3.1	3.4	4.6	0.7	2.8	3.3	2	5.5	4.1	2.2	3
Tb	0.8	0.4	0.5	0.5	0.5	0.7	0.1	0.4	0.5	0.3	0.9	0.6	0.3	0.4
Dy	4.7	2.7	3.1	2.7	2.7	4.4	0.8	2.5	3.2	2	5.3	3.7	1.8	2.4
Ho	0.9	0.6	0.7	0.6	0.6	0.9	0.2	0.5	0.6	0.4	1	0.7	0.3	0.5
Er	2.7	1.6	2	1.7	1.7	2.6	0.7	1.5	1.9	1.3	3.2	2.2	1	1.4
Tm	0.41	0.27	0.32	0.25	0.26	0.39	0.13	0.22	0.29	0.21	0.48	0.33	0.16	0.22
Yb	2.8	1.9	2.2	1.8	1.8	2.6	1.1	1.6	2	1.6	3.3	2.1	1.2	1.5
Lu	0.42	0.3	0.35	0.28	0.29	0.37	0.21	0.27	0.31	0.26	0.52	0.31	0.18	0.22
Hf	4.6	3.5	3.9	3.4	3.1	3.7	1.7	2.9	3.9	3	5.1	3.7	2.3	3.6
Ta	1	0.8	1	0.9	1.2	0.9	1.2	0.5	0.5	1.1	1.3	0.6	0.4	1.1
Tl	0.2	1.1	0.4	0.2	0.3	0.6	0.5	0.2	0.2	0.4	0.6	0.3	0.1	0.3
Pb	5	11	b.l.d.	b.l.d.	b.l.d.	12	17	b.l.d.	12	20	15	8	b.l.d.	8
Th	9.1	6.6	14.7	7.3	6	6.9	16.6	4.7	4.7	9.7	29.5	4.4	4.1	6.2
U	2.4	2.2	2.6	1.5	1.8	2.6	2.4	1.6	1.8	2.1	6.1	0.4	1.6	1.3
Sr/Y	39.7	19.7	7.6	31.6	30.7	16.8	17.7	42.3	29	24.0	12.3	23.1	65.7	30.1
La/Yb$_{(N)}$	10.7	7.8	7.2	10.5	8.2	5.6	5.6	7.8	5.7	10.5	8.8	5.4	11.0	11.0
Eu/Eu*	0.86	0.92	0.69	0.89	0.82	0.71	1.1	0.92	0.92	0.97	0.92	0.88	1.06	0.82

Notes: Major elements in wt%, normalized to 100. Trace elements in ppm. FeO* is total iron expressed as FeO. A/CNK is molar $Al_2O_3/(CaO+Na_2O+K_2O)$. Eu/Eu* is chondrite normalized Eu divided by chondrite normalized (Sm+Tb)/2. b.l.d.—below the limits of detection. All samples are from southern California, USA.

TABLE 3. WHOLE ROCK Sr-Nd ISOTOPE DATA

Sample	$^{87}Rb/^{86}Sr$	$^{87}Sr/^{86}Sr$ (present)	$^{87}Sr/^{86}Sr_i$ (initial)	$^{147}Sm/^{144}Nd$	$^{143}Nd/^{144}Nd$ (present)	$^{143}Nd/^{144}Nd_i$ (initial)	$\varepsilon Nd_{(t)}$	Age (Ma)
El Paso Mountains								
CCQM-1	0.182707	0.705212	0.704559	0.114795	0.512497	0.512308	−0.13	251
MCPF	1.288952	0.709919	0.705225	0.124362	0.512442	0.512234	−1.46	256
GF	1.418401	0.712908	0.707362	0.134495	0.512267	0.512025	−5.06	274
PWM-1	0.201181	0.704926	0.704190	0.118285	0.512599	0.512399	1.8	257
PWM-2	0.316014	0.705855	0.704691	0.136501	0.512486	0.512255	−0.96	259
TRBS-1	0.837550	0.706488	0.703581	0.128771	0.512704	0.512498	3.41	244
TRBS-2	0.708554	0.708711	0.706282	0.149655	0.512653	0.512417	1.74	239
MCP-1	0.156121	0.704157	0.703586	0.110620	0.512646	0.512460	2.98	258
LCP-1	0.290587	0.704828	0.703838	0.140265	0.512734	0.512514	3.60	240
LCP-2	0.579456	0.705952	0.703961	0.106558	0.512648	0.512479	2.98	242
LMT-1	1.015642	0.710992	0.708458	0.112938	0.512065	0.511935	−9.30	176
Fremont Peak								
FPG-1	0.319680	0.707460	0.706233	0.140736	0.512377	0.512128	−3.16	270
Lane Mountain								
LM-1	0.141235	0.705266	0.704758	0.154706	0.512613	0.512357	0.87	253
LM-4	0.359649	0.706565	0.705804	0.105363	0.512436	0.512334	−2.19	149

Note: All samples are from southern California, USA.

2009). Rb-Sr and Sm-Nd data are summarized in Table 3.

RESULTS

Fourteen samples were collected for U-Pb zircon dating from the EPM and northern Mojave regions. Intrusions in the EPM range from small stocks (~500 m radius) to large (> 10 km²), relatively homogeneous bodies occupying up to ~30% of the strike distance of the range (Fig. 2). Samples MCPF, CCQM-1 and MCP-1 are from small plutons that intrude early Paleozoic "eugeoclinal" metasedimentary rocks. Geologic relations of all other plutons to country rocks in the area are uncertain. Most intrusions are medium grained and equigranular with fabrics varying from undeformed to strongly foliated (Figs. 3A, 3B). Pluton compositions are variable, though monzonites and granodiorites are most common. In many of the EPM intrusions, hornblende is altered to chlorite or epidote and sericitic alteration of plagioclase is common (Fig. 3C).

Zircon U-Pb Geochronology

Weighted mean zircon U-Pb ages range from 274 to 239 Ma (Table 1; Fig. 4), allowing us to extend the record of early arc magmatism by ~15 m.y. in this part of the North American Cordillera. Although the Permo–Triassic plutons are the main focus of this paper, two Jurassic plutons were also investigated and are presented for regional framework purposes. Most zircon grains are prismatic, with internal oscillatory

and/or sector zoning textures (Fig. 5) and individual U-Pb analyses generally yield concordant U-Pb ages (Fig. 6). Although inherited components are rare, samples CCQM and MCPF, collected from Late Permian plutons in the EPM, contain between 1 and 5 grains with ages ranging from 0.4 to 2.8 Ga (see Figure 6 and Table DR1 [see footnote 1]). Zircon inheritance in most cases was identifiable in cathodoluminescence (CL) images as chemically distinct interior zones with morphologies not related to the external crystal form (Figs. 5A, 5B). Sample LM-1, collected from a quartz diorite in the Lane Mountain region, yielded zircons with homogeneous patches developed along the margins of oscillatory-zoned grains. Because those patches have low U/Th ratios (~3) and agree well with the ages of nearby dated plutons (ca. 150 Ma), they are interpreted as overgrowths relating to a later magmatic event.

Sample TRBS-2, which was collected from one of many large, leucocratic pods that intrude the darker and more mafic Triassic Burro Schmidt quartz diorite, yielded complex zircon U-Pb ages. Of the 23 zircons analyzed, 6 yielded late Permian to Early Triassic ages ranging between 259 and 250 Ma. The remaining 17 zircons yielded ages ranging from 246 to 234 Ma, with a weighted average of 238.6 ± 1.5 Ma (analytical uncertainty only). We take this average to represent the magmatic age of the leucocratic pods and the older, 259–250 Ma ages to reflect inherited grains. The TRBS-2 sample stands out as not only yielding the most complex U-Pb ages, but also as being the most felsic rock collected and as having a unique REE trend and a more radiogenic initial $^{87}Sr/^{86}Sr$ ratio (discussed in subsequent sections).

Five of the intrusions reported on were previously dated using multi-grain TIMS methods
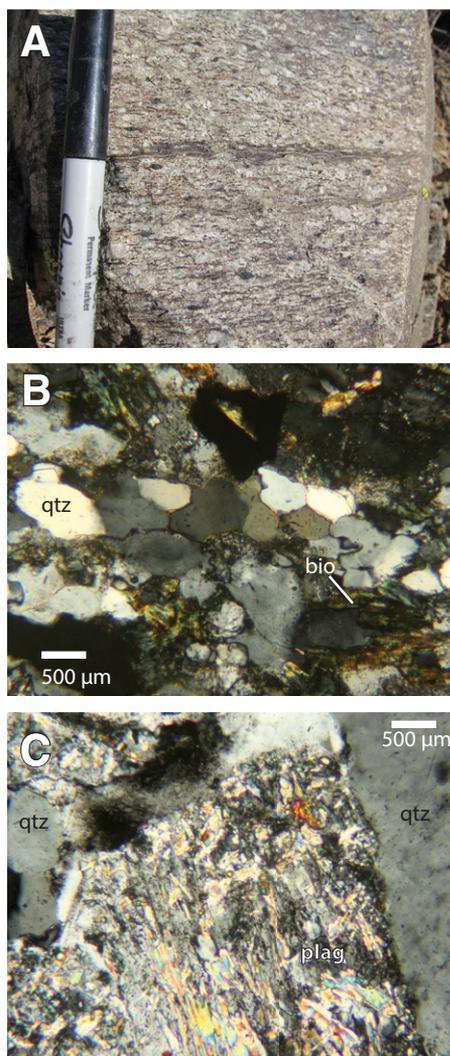
Figure 3. (A) Field photograph of the Permian Weiss Mountain gneiss (sample PWM-2) showing mylonitic fabric. The length of the marker shown in the image is 10 cm. The photograph was taken in Mesquite Canyon, near the contact of the Weiss Mountain gneiss with Paleozoic metasedimentary rocks of the El Paso terrane. (B) Photomicrograph of the deformed Permian granite in the western El Paso Mountains (sample GF). Foliation is defined by bands of recrystallized quartz (qtz) (oriented east-west in the center of the image) and shreddy biotite (bio). (C) Photomicrograph of the undeformed Triassic Last Chance Canyon pluton (sample LCP-1) showing sericitization of plagioclase (plag).
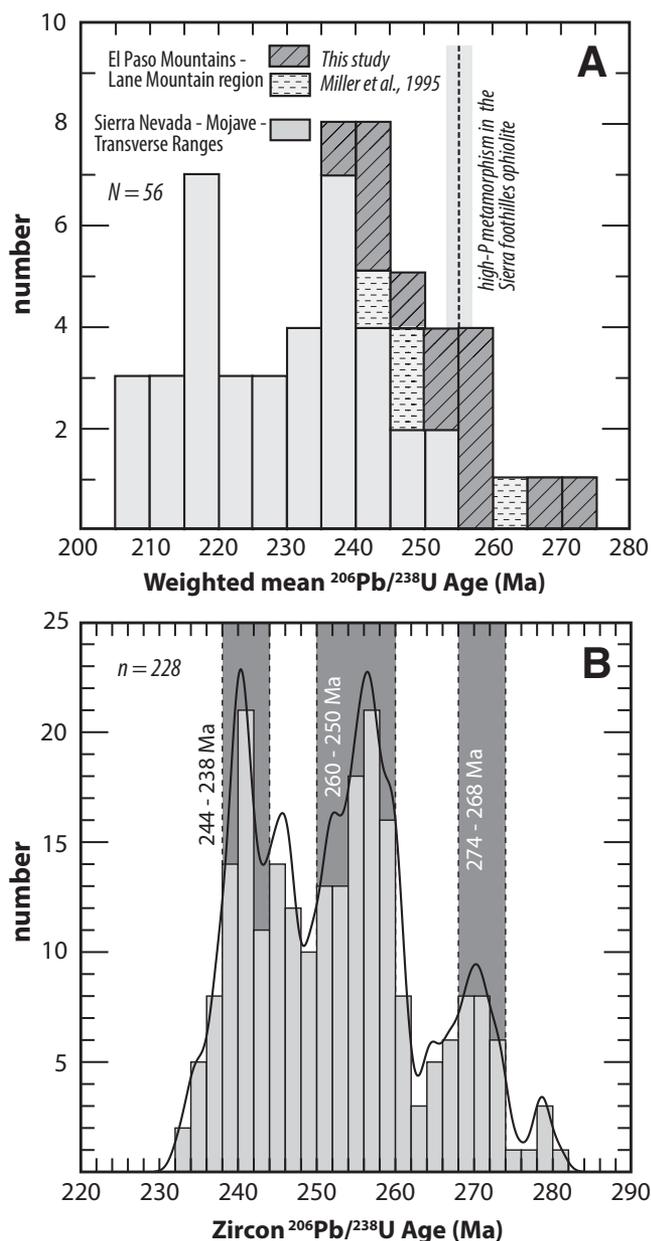
Figure 4. Frequency plots of U-Pb ages. (A) Histogram of all dated Permian and Triassic plutonic rocks from the Sierra Nevada, Mojave, and Transverse Ranges in south-central California, USA (same data sources as for Fig. 1). Timing of high-pressure (high-P) metamorphism recorded in ophiolitic rocks of the Sierra Nevada foothills also shown (Saleeby, 2011). *N*—number of pluton ages included in histogram. (B) Histogram of all zircon grain ages analyzed as part of this study, with kernel density estimate overlain. The distribution of individual ages is used to subdivide our Permian–Triassic data set into three age groups: 274–268 Ma, 260–250 Ma, and 244–238 Ma. Not shown are data from the two Jurassic intrusions discussed herein. *n*—number of individual zircon ages included in histogram.

(Cox and Morton, 1980; Miller et al., 1995). They were re-dated using a single-grain approach as part of this study because of observed discordance likely related to lead-loss and/or zircon inheritance. With the exception of the Weiss Mountain gneiss and the granodiorite pluton of Last Chance Canyon, the new ages presented here are slightly older (by ~6–13 m.y.) than previously interpreted TIMS ages. We note that given the complexity of the zircons, the previously determined bulk ages are in fairly good agreement with the new single-grain ages reported here. Reinterpretation of the ages, however, is significant in that it elucidates temporal trends (e.g., increasing εHf over time) that might otherwise be masked. Based on the distribution of individual zircon U-Pb ages from the studied Permian–Triassic plutons, we define three episodes of magmatism in this part of the northern Mojave at ca. 274–268 Ma, 260–250 Ma, and 244–238 Ma (Fig. 4B). Geochemical and isotopic data discussed in subsequent sections are divided into age groups based on those apparent magmatic pulses.

Whole Rock Major and Trace Element Geochemistry

Magmatic rocks of the northern Mojave region are compositionally diverse but can be generally characterized as calcic to calc-alkalic (Fig. 7), largely metaluminous and magnesian to mildly ferroan. Silica content ranges from 58 to 75 weight percent and is not correlated with pluton age or sampling location. Samples with weighted mean ages between 260 and 250 Ma have a more restricted compositional range, but considerable variation exists between all intrusions in our study area. Northern Mojave Permian–Triassic plutons have Al_2O_3 contents >15%, K_2O between 1.5 and 4%, and Na_2O between 3 and 5% (Table 2) and are broadly similar in major element oxide composition to intermediate to felsic Phanerozoic continental batholiths (e.g., Ducea et al., 2015a).

Trace element compositions show strong large ion lithophile element (LILE) enrichments, with Rb and Ba concentrations >100x more enriched than normal mid-ocean ridge basalt and marked depletions in the high field strength elements (HFSE) Nb, P, and Ti (Fig. 8A). Chondrite-normalized rare earth element (REE) patterns show light-REE enrichments, moderately steep light-REE slopes (La/Sm_N = 3–6), and flat heavy-REE slopes (Dy/Yb_N <1.2) (Fig. 8B). Most sampled plutons have weak, negative europium anomalies (Eu/Eu* = 0.7–1.0). Normalized La/Yb ratios are relatively low (<15) across all age groups. Sr/Y ratios vary from 8 to 65 and are generally higher for the
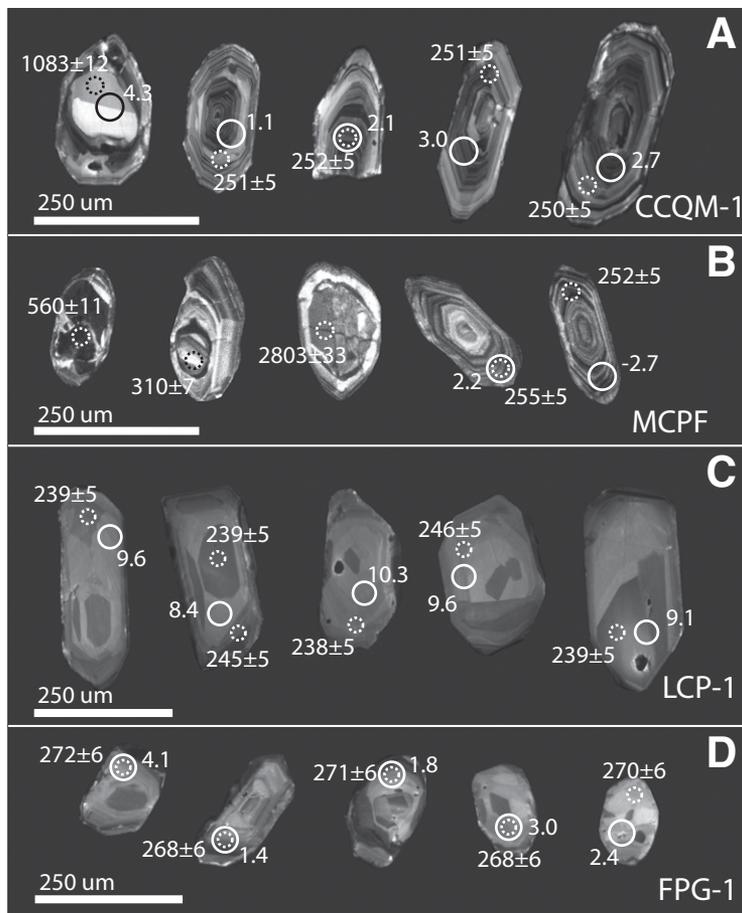
Figure 5. Cathodoluminescence images of zircons showing prismatic morphologies and common textures (oscillatory zonation in A and B; sector zoning in C and D). Inheritance is observed in Permian plutons of the central El Paso Mountains, from which samples CCQM-1 (A) and MCPF (B) were collected. Large, solid circles are locations of Hf isotope analysis spots. Smaller, dashed circles show locations of U-Pb spot analyses. Numbers next to the dashed circles represent analyzed ages, in Ma.

260–250 Ma age group. One outlier in our data set, the highly fractionated leucogranite from the central EPM (sample TRBS-2), is overall more depleted in HFSE and REE, has a very steep light-REE slope (La/Sm_N = 9), a positive heavy-REE slope and a pronounced concavity in the middle REE. In general, however, we observe little geographic or temporal change in the geochemical signatures of the studied plutons.

Whole Rock Sr-Nd Isotope Geochemistry

Strontium and neodymium isotopes were measured in order to investigate spatial and temporal changes in magma sources and to evaluate the degree to which crustal rocks were incorporated in melts. Initial $^{87}Sr/^{86}Sr$ ratios range from 0.7035 to 0.7073 in Permian–Triassic plutons;

initial εNd values of these plutons range from +3.6 to –5.0 and are inversely correlated with initial $^{87}Sr/^{86}Sr$, as expected (Fig. 9). In general, whole rock Sr-Nd isotopes are most evolved in the oldest, late Permian plutons and become progressively more primitive into the Middle Triassic (Fig. 10). The exception to this is the previously discussed Triassic leucogranite (TRBS-2), which yielded a radiogenic initial $^{87}Sr/^{86}Sr$ ratio of 0.7063. In this sample, the Sr isotopic signature appears decoupled from the Nd and Hf in zircon signatures, which are primitive (+1.74 and +10.3, respectively) (Tables 1 and 3).

The Jurassic Laurel Mountain pluton of the eastern EPM (LMT-1; 176 Ma quartz monzodiorite) is the most evolved of all analyzed samples and has an initial $^{87}Sr/^{86}Sr$ ratio of 0.7086 and an initial εNd value of –9.3. By comparison, the Late Jurassic sample from Lane Mountain (LM-4; 149 Ma quartz monzonite) is less evolved with an initial $^{87}Sr/^{86}Sr$ ratio of 0.7058 and an initial εNd value of –2.2.

Zircon Hf Isotope Geochemistry

The samples from this study show significant variation in their zircon initial Hf isotopic compositions ($εHf_{(t)}$), which range from +13 to –9 (Fig. 11; see also Data Repository, footnote 1). Weighted mean averages of zircon $εHf_{(t)}$ values from individual samples range from +10.3 to –0.7 in Permian–Triassic plutons. As documented in the Sr-Nd isotope systematics, zircon $εHf_{(t)}$ also trends toward more primitive values over time, approaching depleted mantle values in the Middle Triassic (Fig. 11). In addition to becoming more primitive, zircon $εHf_{(t)}$ values also exhibit less scatter, becoming more homogeneous over time (Fig. 11). Middle Triassic plutons (244–238 Ma) yield zircons with consistently high $εHf_{(t)}$ values, which range from +6 to +13. In contrast, Permian to Early Triassic plutons (275–250 Ma) yield zircons with highly variable $εHf_{(t)}$ values, ranging from +11 to –9.

As in the case of the Sr-Nd results, the Jurassic Laurel Mountain pluton yields the most evolved zircon εHf signature, with an average $εHf_{(t)}$ of –8.1 (Table 1). In contrast, the Jurassic sample from Lane Mountain (LM-4; 149 Ma quartz monzonite), though somewhat more evolved than older plutons in the area, has an average $εHf_{(t)}$ of +2.7.

DISCUSSION

Onset of Subduction-Related Arc Magmatism

Prior to the ages reported in this study, the earliest documented arc plutonism in this part of the southwestern Cordilleran margin occurred at ca. 260 Ma, the age of the Weiss Mountain orthogneiss in the central EPM (Miller et al., 1995). Saleeby and Dunne (2015) reinterpret the crystallization age of the Weiss Mountain gneiss to be a more precise 256 ± 1 Ma by selecting only the most highly concordant, airabraded fraction, and take that to reflect the onset of subduction-related magmatism along the southwestern margin of Laurentia. This is supported by: (1) continuous, and increasingly voluminous magmatism post 256 Ma and (2) coincident high-pressure metamorphism of mafic mélange blocks that are part of ophiolitic exposures in the southwestern Sierra Nevada at ca. 255 Ma (Saleeby and Sharp, 1980; Saleeby, 2011). We re-dated the Weiss Mountain gneiss in an effort to more accurately date the earliest
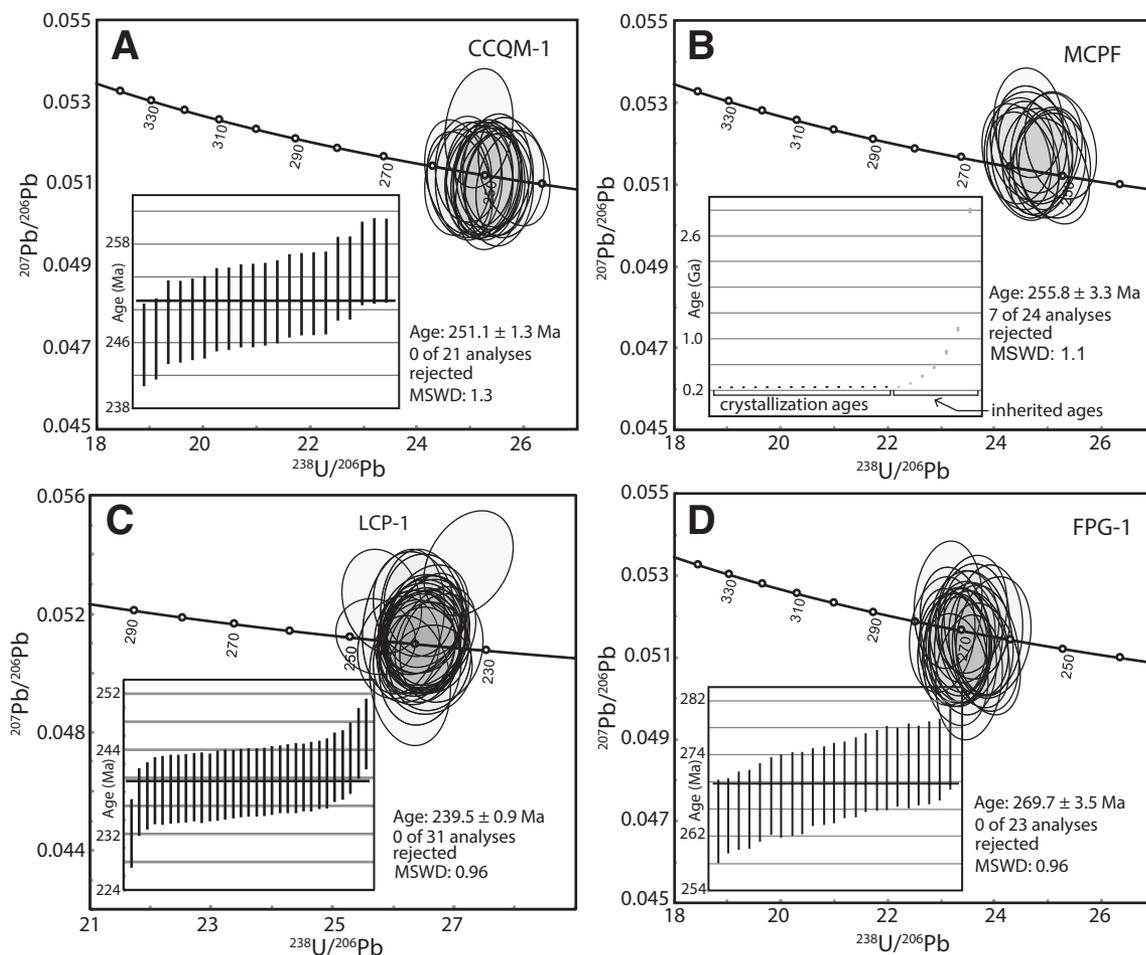
Figure 6. Concordia diagrams and weighted mean plots for the analyzed plutons shown in Figure 5. Samples CCQM-1 (A), MCPF (B) and LCP-1 (C) were collected from the central El Paso Mountains; sample FPG-1 (D) was collected from the Fremont Peak region of the northern Mojave Desert. The ca. 1.1 Ga inherited grain analyzed in sample CCQM is not shown. Error ellipses and error bars are shown at 95% confidence interval. Gray bars in the weighted mean plots are analyses that are not included in the calculation of the weighted mean age. Ages shown are weighted mean ages of the selected analyses with combined systematic and analytical errors at 2s. MSWD—mean square of weighted deviates.

arc magmatism in the region and to investigate the presence and/or age of possible inheritance, suggested by the discordance of the Miller et al. (1995) bulk zircon age. We dated the unit near its western margin, where is it relatively undeformed (257.2 ± 3.3 Ma), and on its eastern margin (258.5 ± 3.3 Ma), where it develops a mylonitic fabric. We also targeted other similarly deformed plutons, two of which yielded ages demonstrably older than the Weiss Mountain. One of these bodies, a foliated granite in the western EPM (sample GF) yielded 11 concordant zircon analyses with a weighted mean age of 273.7 ± 4.4 Ma. Another, an orthogneiss near Fremont Peak (sample FPG-1), yielded 23 concordant zircon analyses with a weighted mean age of 269.7 ± 3.5 Ma. In contrast to Miller et al.

(1995), we did not find evidence for inheritance in our single-grain dating of this unit.

Data from the early Permian Fremont Peak gneiss and the western EPM foliated granite suggest that subduction initiated significantly earlier than previously recognized. Although we know of no other intrusive units of this age in this part of the southwestern Cordillera, Permian metavolcanic rocks are documented in the area. Martin and Walker (1995) report an upper intercept age of 281 ± 8 Ma for an andesite flow in the western EPM. Chapman et al. (2012) report an age of 273 ± 2.4 Ma for a dacitic metatuff in the Bean Canyon pendant of the southern Tehachapi Mountains. The age and trace element geochemistry of Permian felsic metavolcanic rocks in the Bean Canyon pendant are similar

to that of the foliated granite in the western EPM (sample GF), suggesting a possible relationship. Furthermore, ca. 280–270 Ma detrital zircon grains have recently been documented in Permo–Triassic strata of the EPM, Lane Mountain region and southern Inyo Mountains (McDonald et al., 2016; Riggs et al., 2016a: Brown et al., 2018). Although the Cretaceous overprint is significant everywhere in the Cordilleran arc, the fact that Permian magmatism has only been recognized in few pendants preserved in the southern Sierra Nevada/northern Mojave region indicates that early arc magmatism is unique to that area.

Permian plutonism has also been documented farther south along the plate margin in Sonora, Mexico. Riggs et al. (2009) report a Permian
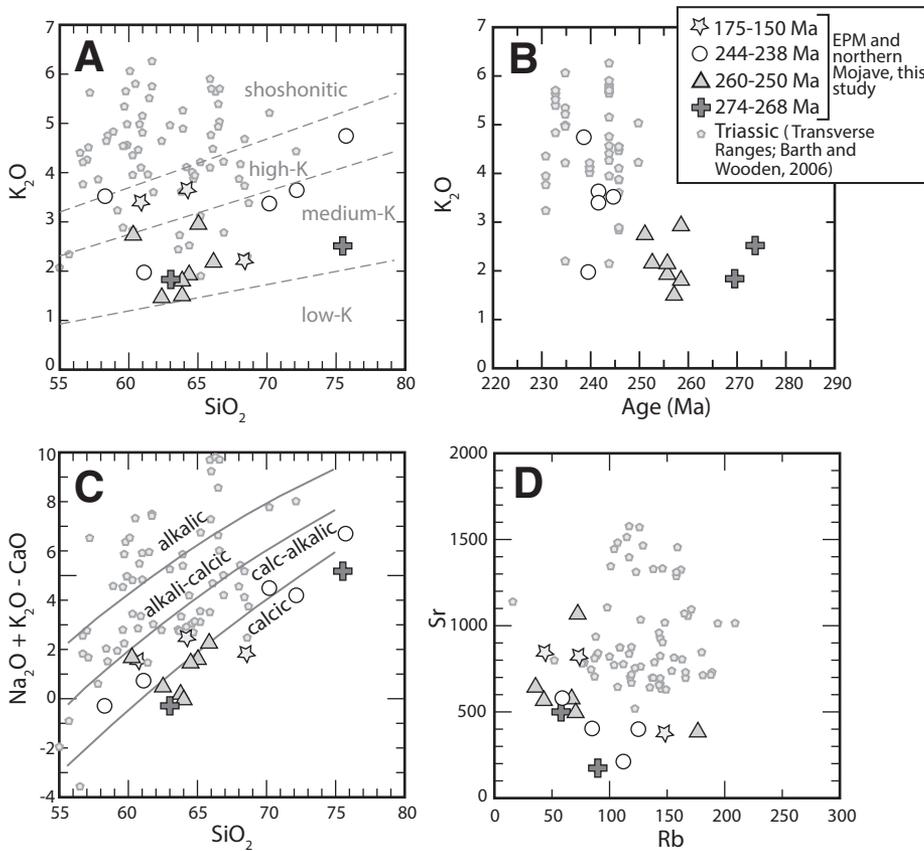
Figure 7. Whole rock geochemical variation diagrams for plutons of the El Paso Mountains (EPM) and northern Mojave Desert region, south-central California, USA (this study and data from three samples reported in Miller et al., 1995), compared with data from partially coeval intrusive suites of the Transverse Ranges and central Mojave (Barth et al., 1990). Major element oxide concentrations are in wt%; trace element concentrations are in ppm. (A) Plot of K_2O vs SiO_2 showing the highly potassic to shoshonitic character of the Triassic suites to the south and east of our study area. (B) Plot of K_2O vs age showing an apparent trend toward increasing K_2O through time, suggesting a temporal and/or spatial shift in magma source. (C) Plot of $Na_2O + K_2O – CaO$ vs SiO_2 showing the difference between calcic to calc-alkaline plutons of the northern Mojave region and the alkali-calcic to alkalic nature of Transverse Ranges and central Mojave plutons. (D) Plot of Sr vs Rb concentrations illustrating relative enrichment of both elements in the Triassic arc of the Transverse Ranges.

age (270 Ma) for a granitic pluton in the Sierra Los Tanques region of northern Sonora. Arvizu and Iriondo (2015) report crystallization ages ranging from 257 to 224 Ma for the Los Tanques region intrusive suites and pluton ages as old as 275 Ma for the nearby Sierra Pinta region (Ar-

vizu et al., 2009). Permo–Triassic magmatism in northern Sonora is distinct from coeval magmatism in the northern Mojave region in that Sonoran magmas intrude and interact with Proterozoic basement, as documented in field studies and abundant Proterozoic inherited zircon

populations (Arvizu and Iriondo, 2015). The Sonoran Permo–Triassic also has much more evolved Hf and Nd isotopic signatures (average zircon εHf = –7.4 and whole rock εNd = –11.2 versus εHf = 0 and εNd = –5 for northern Mojave magmas; Riggs et al., 2016b) (Fig. 9). It
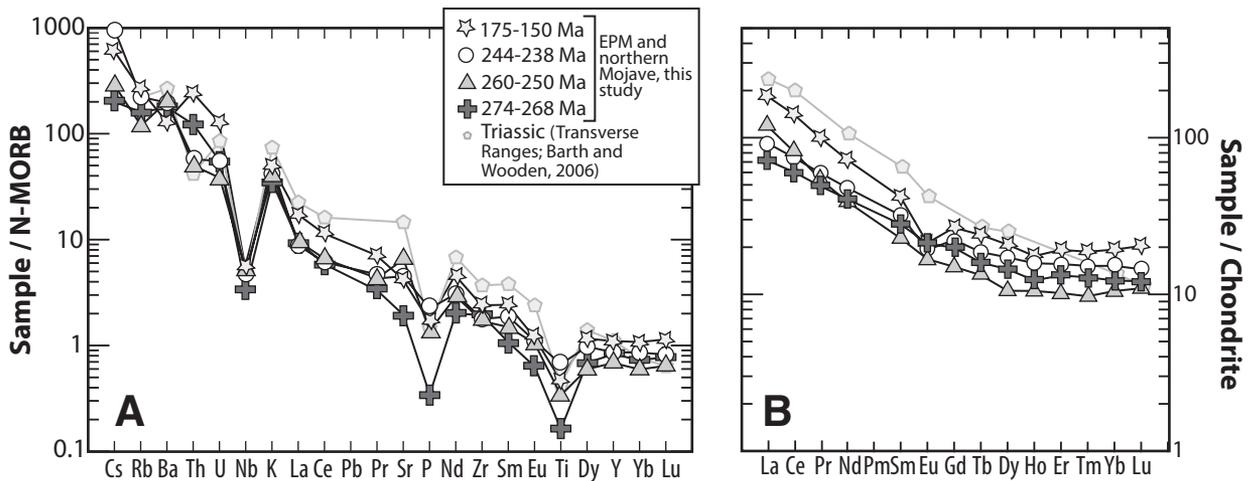
Figure 8. (A) Normal mid-ocean ridge basalt (N-MORB) normalized trace element abundance diagrams, and (B) rare earth element abundances normalized to chondrite values (Sun and McDonough, 1989). Representative samples from the El Paso Mountains for each age group were plotted. Same symbols and data sources as in Figure 7. EPM— El Paso Mountains.
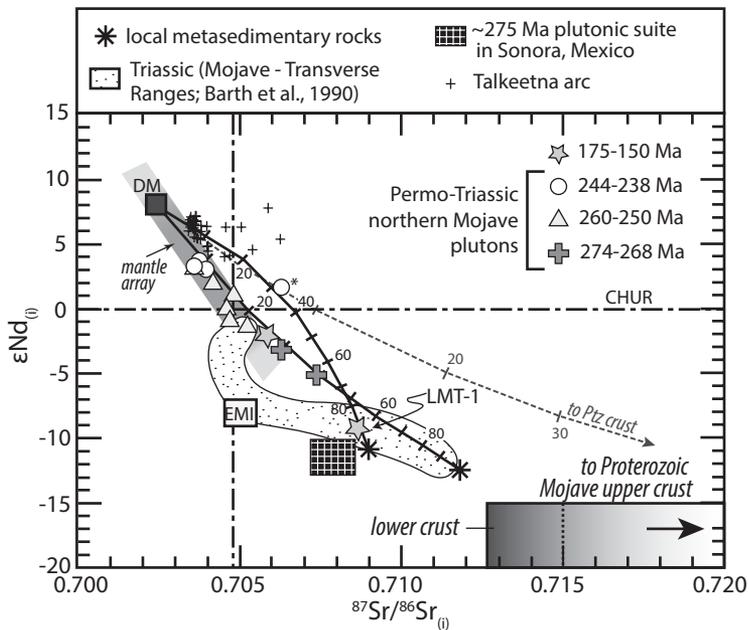
Figure 9. Initial $^{87}Sr/^{86}Sr$ versus initial ε_{Nd} for Permian–Jurassic plutons of the El Paso Mountains and central Mojave region, south-central California, USA. For comparison, Sr-Nd fields for Triassic plutons of the Transverse Ranges (Barth et al., 1997; Barth and Wooden, 2006), the Permian Los Tanques plutonic suite in northern Sonora, Mexico (Riggs et al., 2016b), and the Talkeetna intra-oceanic arc, south-central Alaska, USA, (Rioux et al., 2007) are also shown. Lines represent mixing trajectories of depleted mantle with "eugeoclinal" Paleozoic metasedimentary rocks of the Goldstone region (central Mojave) from Miller and Glazner (1995), though we note that any assimilation and fractional crystallization process could produce arrays not predicted by the simple mixing models discussed. The mantle end-member has 113 ppm Sr, $^{87}Sr/^{86}Sr$ (250 Ma) = 0.7027, 11 ppm Nd, ε_{Nd} (250 Ma) = +8 (Workman and Hart, 2005). The metasedimentary end-members have 209 ppm Sr, $^{87}Sr/^{86}Sr$ (250 Ma) = 0.71191, 28 ppm Nd, ε_{Nd} (250 Ma) = –12.7 and 306 ppm Sr, $^{87}Sr/^{86}Sr$ (250 Ma) = 0.70912, 13 ppm Nd, ε_{Nd} (250 Ma) = –11 (Miller and Glazner, 1995). Gray dashed trajectory represents mixing of depleted mantle with Mojave continental crust (average of upper and lower Proterozoic Mojave crust from Miller et al., 2000). Sample represented by white circle with an asterisk next to it is a high SiO_2 leucocratic pod in the Triassic Burro Schmidt pluton. CHUR—chondritic uniform reservoir; DM—depleted mantle reservoir; EMI—enriched mantle I; Ptz—Proterozoic.

is therefore unlikely that Sonoran and northern Mojave magmas were cogenetic and later displaced along the putative Mojave Sonora megashear or other strike slip fault system. Taken together, it appears that subduction may have nucleated simultaneously at two locations along the southwestern Laurentian margin in Permian time before developing into a more regionally extensive Triassic magmatic arc.

Partially coeval (ca. 250–215 Ma) plutons from the central Mojave and Transverse Ranges record a northwest to southeast younging of magmatism across the region (Barth et al., 1997; Barth and Wooden, 2006). Intrusive rocks of the EPM and northern Mojave are generally older than, and located northwest of, the Triassic suites, supporting the pattern of a southward progression in magmatism. Triassic plutons of the central Mojave and Transverse Ranges differ significantly from EPM and northern Mojave plutons, however, in the following ways: (1) they intrude Proterozoic basement and its cratonal/ miogeoclinal cover, (2) they contain large populations of Proterozoic inherited zircons, (3) they exhibit evolved isotopic characteristics (Fig. 10), and (4) they have distinctive mineralogy and geochemistry in that they tend to be quartz poor, enriched in FeO and K_2O (commonly shoshonitic), calc-alkalic to alkalic, and have characteristically high Sr concentrations (>600 ppm) (Fig. 7). These differences suggest that the Triassic plutons, although partially overlapping in time and space with the EPM and
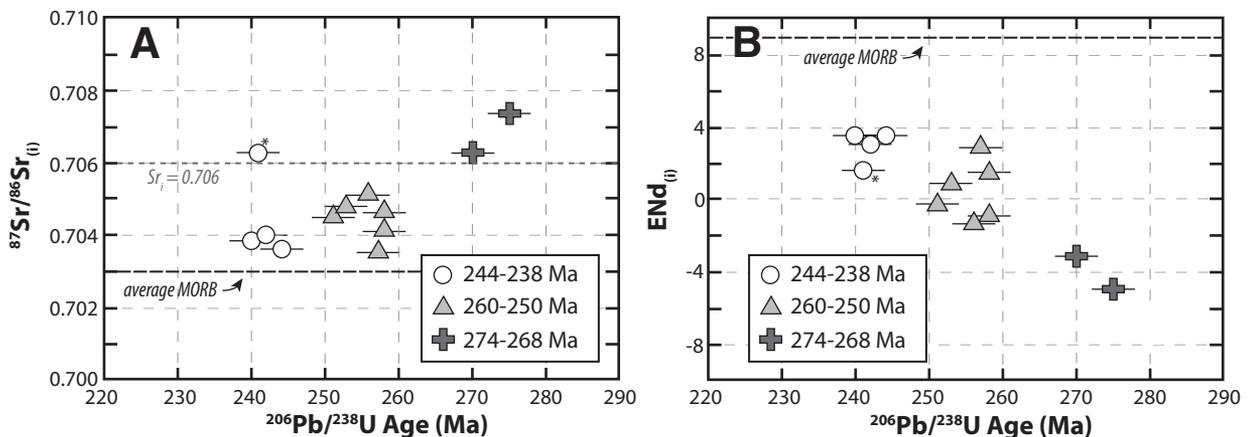
Figure 10. Initial $^{87}Sr/^{86}Sr$ (A) and initial ε_{Nd} (B) versus age for plutons of the El Paso Mountains and central Mojave region, south-central California, USA, highlighting trends toward more primitive isotopic values over time. Sample represented by white circle with an asterisk next to it is a high SiO_2 leucocratic pod in the Triassic Burro Schmidt pluton. Average Sr_i and ε_{Ndi} of mid-ocean ridge basalt (MORB) from White (2010). Vertical errors are smaller than the sample polygons shown.

Figure 11. Plot of zircon εHf(t) versus age for Permo–Triassic plutons of the El Paso Mountains and central Mojave region, south-central California, USA, plotted as a function of whole rock SiO₂ content. CHUR—chondritic uniform reservoir.

zircon inheritance observed in two EPM plutons and is common among early Cordilleran arc sequences (Wetmore and Ducea, 2011; Walker et al., 2015). Lastly, we note that EPM and northern Mojave intrusives have isotopic signatures that are considerably more evolved than most island arcs that are emplaced into oceanic lithosphere. Intermediate plutonic rocks of the Talkeetna arc, south-central Alaska, USA, a classic example of an accreted intra-oceanic arc, typically yield age-corrected Sr ratios <0.705 and εNd > +5 (Rioux et al., 2007) (Fig. 9).

Whole rock Sr-Nd values are negatively correlated, forming a generally linear array. Results from simple binary mixture models indicate that the isotopic composition of these melts can be explained by 2-component mixing of depleted mantle and local eugeoclinal Paleozoic metasedimentary (argillaceous) rocks (Miller and Glazner, 1995) (Fig. 9). These metasedimentary end-members were chosen because they are proximal to our study area and several plutons in the EPM are observed to intrude similar rocks. Modeling indicates that the relative contribution of supracrustal metasedimentary rocks into the earliest melts (274–268 Ma) could be as high as 30%–40%, while Triassic magmas (244–238 Ma) could be produced by mantle melts with <10% mixing of supracrustal material (Fig. 9). Contributions from metasedimentary rocks could be considerably lower if a more enriched mantle end-member is chosen. At present, oxygen isotope data is not available to evaluate the contamination by sedimentary material of early arc plutons in the region. Intrusive rocks with a similar range of isotopic values in the Idaho batholith were best fit by models invoking mixing of mantle with lower crustal gneisses (Fleck and Criss, 1985; Fleck, 1990). Contamination by an enriched and/or older crustal component is permitted by our data, though mixing trajectories between depleted mantle and limited available data for Proterozoic Mojave crust (upper and lower; Miller et al., 2000) were not found to be good fits (Fig. 9).

The Early Jurassic Laurel Mountain pluton of the eastern El Paso Mountains is notably more evolved (initial ⁸⁷Sr/⁸⁶Sr ratio = 0.7085; initial εNd = 9.3) than the Permo–Triassic suite and has been interpreted as intruding Precambrian North American basement (Miller et al., 1995; Saleeby and Dunne, 2015). Given that Jurassic plutons in the nearby Lane Mountain region have considerably more primitive isotopic characteristics, the evolved nature of the Laurel Mountain pluton likely reflects a spatial, and not temporal, variation. Intrusion of the Laurel Mountain pluton into distinctly different crust than that of the Permo–Triassic plutons in the central and western EPM indicates that the

northern Mojave rocks described herein, have very different magma sources. Compositional differences, and differences in source rock character, could be ascribed to the varying basement domains into which the plutons are intruded (El Paso terrane basement in the case of the EPM-northern Mojave intrusions and Proterozoic continental crust in the case of the central Mojave-Transverse Ranges intrusions). It's also possible that there was a temporal shift to partial melting of distinct source rocks across this region in Early to Middle Triassic time, as suggested by an increase in the K₂O of Triassic plutons in the EPM and northern Mojave (Fig. 7).

Early Arc Petrogenesis

Permo–Triassic plutons of the EPM and northern Mojave region are unique in that they are older than most other intrusive suites documented for the southwestern Laurentian margin, and they mostly intrude the somewhat cryptic El Paso terrane, whose nature and allochthoneity is not well constrained. Whole rock Sr-Nd signatures and Hf isotopes in zircon were analyzed to identify spatio-temporal patterns of arc development, if present, and to assess the relative contributions of crust and mantle in generating early arc products. The Sr-Nd signatures observed in plutons of the EPM and northern Mojave region are variable but are generally more primitive than those documented for partially coeval

intrusive suites of the Transverse Ranges and central Mojave (Fig. 9). Permo–Triassic plutons in the EPM are observed to intrude eugeoclinal (deep water) facies rocks, but the basement underlying those sediments, if there was any, is unknown. This is not unusual among early arc exposures in the Pacific realm (e.g., Ducea et al., 2017) or beyond; many miogeoclinal sections appear to have been thick sequences of passive margin sediments resting on highly attenuated or no continental basement. Rare exposures of greenstones with pillow textures are associated with eugeoclinal strata in the EPM and in the Pilot Knob area to the east (Carr et al., 1984, 1992), suggesting that the basement to the El Paso terrane, at least in some areas, may be oceanic basaltic crust. The Permo–Triassic plutons investigated herein, however, are difficult to reconcile with derivation solely from depleted oceanic lithosphere given their highly fractionated nature (up to 75% SiO₂), their variable, but moderately evolved Sr-Nd signatures (Srᵢ up to 0.708, initial εNd as low as –5, and initial εHf in zircon as low as –9) (Figs. 9–11). Moreover, coeval mafic intrusive rocks are rare in the northern Mojave and EPM region. Initial ⁸⁷Sr/⁸⁶Sr ratios >0.706 and relatively low initial εNd suggests the involvement of either an enriched mantle source or radiogenic continental crust and/or sedimentary materials derived from cratonic North America in magma generation. The latter is supported by limited Precambrian

eastern boundary of the El Paso terrane passes through the central-eastern part of the El Paso Mountains. The nature of that boundary, and whether or not it is a pre-Jurassic thrust that puts deep-water facies rocks underlain by oceanic lithosphere on continental margin rocks, as suggested by Miller et al. (1995), is not resolvable with our data.

Like the Laurel Mountain pluton, Triassic intrusive rocks in the San Gabriel Mountains have enriched Sr isotopic signatures (initial $^{87}Sr/^{86}Sr$ up to 0.711) and highly negative $\varepsilon Nd_{(t)}$ (as low as –11.8), and are consistent with derivation by partial melting of Proterozoic Mojave crust (Barth et al., 1990; Fig. 9). This suggests that Triassic magmatism to the south is likely developing in older, thicker (?) continental lithosphere and that the upper-plate to the early southern Cordilleran arc is complex over relatively small spatial scales.

Temporal and Spatial Variations in Magmatism

Although whole rock compositions are broadly similar among the identified age groups, we observe significant variation through time in all isotopic systems. The oldest rocks in our Permo–Triassic data set, the 274 Ma foliated granite of the western EPM and the 270 Ma Fremont Peak gneiss, yield the most evolved isotopic compositions. Initial $^{87}Sr/^{86}Sr$ in those rocks is >0.706 and they have the lowest recorded initial εNd and initial εHf in zircon values. The foliated granite differs from many of the other studied intrusions in that it is more felsic ($SiO_2 = 75\%$), it is slightly more peraluminous (A/CNK = 1.1), and has an observable negative europium anomaly (Eu/Eu* = 0.7). These geochemical signatures could indicate a greater influence of crustal material in the melt, as suggested by the Sr-Nd isotopic modeling. Plutons that were emplaced during the late Permian (ca. 260–250 Ma) have lower initial $^{87}Sr/^{86}Sr$ (0.7036–0.7052) and higher initial εNd and initial εHf in zircon values. Even more primitive values are observed in Early to Middle Triassic plutons (Figs. 10 and 11).

Early arc magmatism has been observed in many continental arcs to be more isotopically evolved and more fractionated than later melts. That is because arcs typically develop along, or proximal to, long-lived passive continental plate margins and early melts are in part products of melt fertile sedimentary packages in the upper plate (e.g., Ducea et al., 2015a, 2015b). Over time, as the arc becomes more thermally mature and the more fertile sedimentary material becomes depleted, the relative contribution of upper-plate crust is reduced and the isotopic sig-

natures of melts become more mantle-like. This has been documented in the early development of other Cordilleran arc systems including the Coast Mountains batholith, in the Pacific Northwest of North America (Wetmore and Ducea, 2011); the Sierra Nevada batholith, California, USA (Ducea et al. 2015b); and the Famitinian arc in Argentina (Walker et al., 2015). In light of that, the isotopic trends displayed by rocks studied here (earlier rocks are more evolved isotopically) is somewhat typical of initial arc magmatism, at least in the North American Cordillera, and could explain the trends illustrated in Figures 10 and 11.

Changing tectonic conditions in the upper plate during development of the newly convergent margin could also explain observed changes in the isotopic character of the arc melts through time. Recent global plate reconstructions for Paleozoic time suggest near-orthogonal convergence in southwest Laurentia at ca. 270 Ma (Domeier and Torsvik, 2014). Strong convergence at angles near perpendicular to the plate margin during and immediately following subduction initiation would drive contractional tectonism in the upper plate, promoting crustal thickening and a greater contribution of crustal material to melt source regions. Inherited Precambrian and Paleozoic zircons and more evolved isotopic signatures in Permian plutons support this model. Permian plutons, including the synkinematic Weiss Mountain gneiss, also commonly exhibit deformation fabrics (Fig. 3) which are consistent with emplacement in a contractional environment. Permian contractional tectonism has been documented in the region (e.g., Stevens and Stone, 2005), and has been associated with rapid exhumation of newly emplaced plutons (Saleeby and Dunne, 2015). Exhumation and erosion of Permian intrusions during this contractional regime could also explain their scarcity in modern exposures of the Cordilleran arc in the region.

In contrast to the Permian, Triassic plutons appear more voluminous, less deformed and are more widespread and better preserved in the geologic record. They also have higher εNd and zircon εHf, lower Sr_i, and lack inherited zircon populations. A shift toward a more primitive isotopic character could reflect a change to a more depleted mantle source, involvement of a distinct, and less enriched/younger crustal component, involvement of the same components, but with less of the crustal end-member contributing, or a combination of all of these. Though not required by the geochemical or isotopic data, changes in mid-Triassic magmatism could be interpreted to reflect a change in upper-plate stress conditions from a largely compressional to a transtensional or extensional tectonic

regime. This is supported by the development of an arc-graben system and the accumulation of large thicknesses of volcaniclastic strata in marine basins in the southern Cordillera in Late Triassic to early Middle Jurassic time (Busby-Spera, 1984; Saleeby and Busby-Spera, 1992). The generation of Triassic magmas with variable SiO_2 content (58%–76% SiO_2; Fig. 7) but primitive isotopic signatures (e.g., Fig. 11), could indicate a shift toward a bimodal magmatic system, consistent with development of extensional tectonism. A change to a more extensional tectonic mode in the upper plate of a subduction system could be driven by steepening slab dip (e.g., Lallemand et al., 2005) or by a change to a more oblique convergence angle and lower overall convergence velocity (e.g., Zuo et al., 2017). The latter is our preferred model given that a recent plate-velocity model shows a change between ca. 270 and 250 Ma to more oblique convergence along the SW Laurentian margin (Domeier and Torsvik, 2014).

Tectonic Development of the Early Cordilleran Arc

We propose a model of the early Cordilleran arc, as exposed in the EPM and northern Mojave, as developing in a peri-allochthonous sliver of transitional (oceanic to attenuated continental) lithosphere capped by marine slope and rise facies of the passive margin. This sliver—what is now the El Paso terrane—could have been one of the "framework ribbons" of Saleeby and Dunne (2015) that was calved off and displaced by the plate-bounding sinistral fault system that preceded and, was likely synchronous with, the initiation of subduction in the region (Fig. 12A). It is also possible that the El Paso terrane formed outboard of its present location and was subsequently thrust against the continental margin (e.g., Miller et al., 1995). Both scenarios could account for the juxtaposition of deep-water facies against shelf facies of the miogeocline to the east and are unresolvable with our data. As plate vectors changed toward more convergent tectonism, outboard slivers of the distal passive margin would have been sutured onto the SW continental margin forming a heterogeneous upper plate to a newly initiated subduction zone (Fig. 12B). We argue that this occurred at ca. 275 Ma at the latitude of the central/northern Mojave block. The relatively evolved isotopic signatures of the Permian plutons documented herein argue against their having developed in an off-shore fringing island arc system and later accreted to the margin, as in the case of the Talkeetna arc (Fig. 9). The late early Permian presumably would have also been the approximate time of docking of the Caborca block in Sonora,
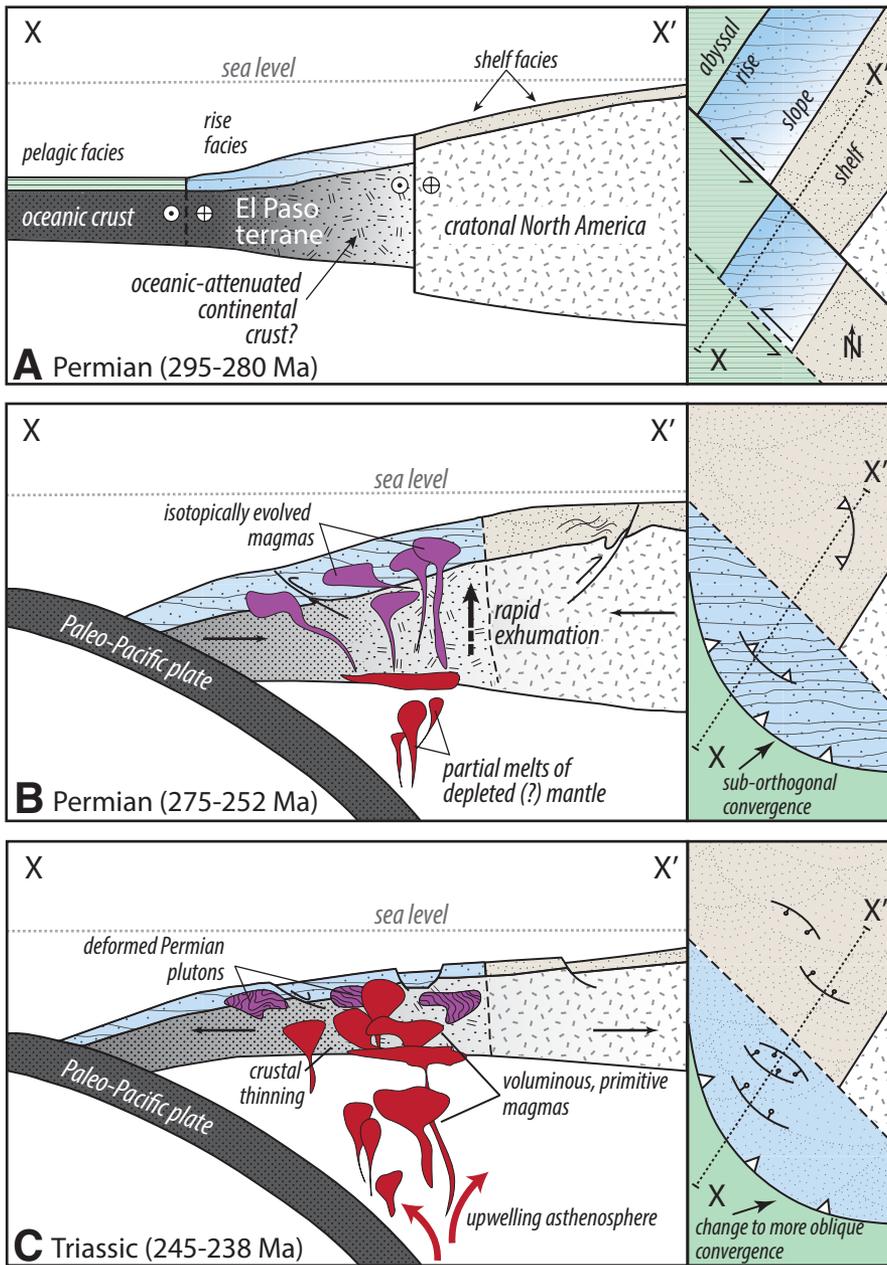
Figure 12. Schematic cross sections (A–C) for the Permian–Triassic at the latitude of northern Mojave, California, USA. Boxes to the right of each cross section show proposed plate reconstructions for each time interval. Part (A) shows the translation (?) and tectonic juxtaposition of the El Paso terrane against the continental margin prior to subduction initiation. Part (B) shows the period following subduction initiation, which is marked by the development of moderately evolved plutons that are deformed and rapidly exhumed in a contractional setting. Part (C) shows the proposed switch to more oblique convergence that puts the upper plate into extension and leads to the development of more primitive, primarily mantle-derived melts.

Mexico and the initiation of the Cordilleran arc there (e.g., Riggs et al., 2014; Arvizu and Iriondo, 2015). The strike of the NW-trending off-shore slivers, or ribbons, would have been oblique to the continental margin and to convergence vectors, such that other slivers (e.g., the Kernville terrane) would have accreted at later times, as evidenced by the later onset of magmatism in the southern Sierra Nevada.

As subduction initiated and flux melting began in the upper plate, the first magmas would have been derived from mantle, likely contaminated at depth by more radiogenic and/or older continental basement or during ascent by partial melting of fertile passive-margin sedimentary rocks. Contractional deformation active during emplacement of these early magmas may have enhanced crustal contributions to the melts and generated the magmatic fabrics seen in several of the Permian plutons. This may be a signal common to early arcs developing at convergent margins that undergo forced subduction initiation. Although very few middle Permian magmatic products are exposed today, their erosional equivalents have been documented in the detrital zircon spectra of Permian metasedimentary rocks of the EPM and Lane Mountain region (McDonald et al., 2016; Brown et al., 2018) and in Triassic backarc strata of the Colorado Plateau, USA (Riggs et al., 2013; 2016a). A switch in the upper-plate stress state from compression to extension was likely driven by the rotation of plate vectors to a more oblique orientation (Domeier and Torsvik, 2014). This may have promoted asthenospheric upwelling and more vigorous mantle-sourced magmatism, leading to the production of larger, undeformed intrusions with more primitive isotopic signatures (Fig. 12C). It is also possible that this contributed to the generation of regional potassic magmatism in Middle to Late Triassic time (Fig. 7), which has been attributed in some settings to intra-arc extensional tectonism (Stern et al., 1988; Bloomer et al., 1989; Lange and Carmichael, 1991). Overall, the pulsed nature of early arc magmatism and significant changes in the isotopic character of early melts suggests that evolution of the nascent subduction zone was tectonically complex, as was the spatial and temporal development of the early magmatic arc.

CONCLUSIONS

New pluton geochronology, combined with geochemical and isotopic signatures from the EPM and northern Mojave region, provide important constraints on the timing and petrotectonic nature of subduction initiation along the southwest Laurentian margin. The ages

presented here extend the record of subduction-related magmatism back to ca. 275 Ma, some 15–20 m.y. earlier than previously estimated. Age patterns suggest that subduction nucleated in the northern Mojave region and later spread northward into the southern Sierra Nevada and southward to the Transverse Ranges. Felsic intrusive suites with ages similar to 275 Ma have been documented in Sonora, Mexico, indicating that the arc may have had multiple initiation zones before becoming more coherent and widespread in Triassic to Jurassic time. Geochemistry of the northern Mojave Permo–Triassic plutons shows that they are typical of (albeit compositionally diverse) subduction-related Cordilleran arc, but markedly different than partially coeval Triassic plutonic suites of the central Mojave and Transverse Ranges. Trends in the isotopic data toward more primitive values over time may reveal changing tectonic conditions in the upper plate of the nascent subduction zone. Subduction initiation was likely "forced" (Stern, 2004) by a plate kinematic transition from transform to transpressional. As convergence became more perpendicular to the margin early on, the upper plate—composed of a heterogeneous assemblage of accreted tectonic slivers—experienced contractional deformation. This led to crustal thickening and the production of more isotopically evolved melts that incorporated distal Paleozoic passive-margin strata. Over time, plate kinematic changes led to extension in the upper plate and the production of more voluminous, mantle-derived melts.

APPENDIX

Analyses at the University of Arizona were performed on rock powders dissolved in Savillex vials using a mixture of hot concentrated $HF\text{-}HNO_3$ or alternatively, a mixture of cold concentrated $HF\text{-}HClO_4$. The dissolved samples were spiked with a batch of the Caltech "Lunatic Asylum" Rb, Sr, and mixed Sm-Nd spikes (calibrated in Otamendi et al., 2009) after dissolution. Rb, Sr, and the bulk of the REEs were separated in cation columns containing AG50 W-X4 resin, using 1 N to 4 N HCl. Separation of Sm and Nd was achieved in anion column containing LN Spec resin, using 0.1 N to 2.5 N HCl. Rb was loaded onto single Re filaments using silica gel and H_3PO_4. Sr was loaded onto single Ta filaments with Ta_2O_5 powder. Sm and Nd were loaded onto single Re filaments using platinized carbon, and resin beads, respectively. Mass spectrometric analyses were carried out on an automated VG Sector multicollector and a VG Sector 54 instrument fitted with adjustable 10^{11} W Faraday collectors and a Daly photomultiplier (Otamendi et al., 2009). Concentrations of Rb, Sr, Sm, and Nd were determined by isotope dilution, with isotopic compositions determined on the same spiked runs. Typical runs consisted of acquisition of 100 isotopic ratios. The mean result of ten analyses of the standard NRbAAA performed during the course of this study is: $^{85}Rb/^{87}Rb = 2.6123 \pm 20$. Fifteen analyses of standard Sr987 yielded mean ratios of: $^{87}Sr/^{86}Sr = 0.710265 \pm 7$ and $^{84}Sr/^{86}Sr = 0.056223 \pm 12$. The mean results of

five analyses of the standard nSmb performed during the course of this study are: $^{148}Sm/^{147}Sm = 0.74882 \pm 21$ and $^{148}Sm/^{152}Sm = 0.42130 \pm 6$. The estimated analytical uncertainties are: $^{87}Rb/^{86}Sr = 0.36\%$ (2σ), $^{87}Sr/^{86}Sr = 0.0011\%$ (2σ), $^{147}Sm/^{144}Nd = 0.38\%$ (2σ), and $^{143}Nd/^{144}Nd = 0.0011\%$ (2σ). Procedural blanks averaged from five determinations were: Rb-11 pg, Sr-120 pg, Sm-2.8 pg, and Nd-5.7 pg. The Sr isotopic ratios were normalized to $^{86}Sr/^{88}Sr = 0.1194$, Nd isotopic ratios were normalized to $^{146}Nd/^{144}Nd = 0.7219$.

REFERENCES CITED

Arvizu, H.E., and Iriondo, A., 2015, Temporal and geologic control of Permo-Triassic magmatism in Sierra Los Tanques, NW Mexico: Evidence of the initiation of cordilleran arc magmatism in SW Laurentia: Bulletin of the Geological Society of Mexico, v. 67, p. 545–586.

Arvizu, H.E., Iriondo, A., Izaguirre, A., Chavez-Cabello, G., Kamenov, G.D., Solis-Pichardo, G., Foster, D.A., and Lozano-Santa Cruz, R., 2009, Rocas graniticas permicas en la Sierra Pinta, NW de Sonora, Mexico: Magmatismo de subduccion asociado al inicio del margen continental activo del SW de Norteamerica: Revista Mexicana de Ciencias Geológicas, v. 26, p. 709–728.

Barth, A.P., and Wooden, J.L., 2006, Timing of magmatism following initial convergence at a passive margin, southwestern US Cordillera, and ages of lower crustal magma sources: The Journal of Geology, v. 114, no. 2, p. 231–245, http://doi.org/10.1086/499573.

Barth, A.P., Tosdal, R.M., and Wooden, J.L., 1990, A petrologic comparison of Triassic plutonism in the San Gabriel and Mule Mountains, southern California: Journal of Geophysical Research, v. 95, no. B12, p. 20075–20096, http://doi.org/10.1029/JB095iB12p20075.

Barth, A.P., Tosdal, R.M., Wooden, J.L., and Howard, K.A., 1997, Triassic plutonism in southern California: Southward younging of arc initiation along a truncated continental margin: Tectonics, v. 16, no. 2, p. 290–304, http://doi.org/10.1029/96TC03596.

Barth, A.P., Wooden, J.L., Coleman, D.S., and Fanning, C.M., 2000, Geochronology of the Proterozoic basement of southwesternmost North America, and the origin and evolution of the Mojave crustal province: Tectonics, v. 19, no. 4, p. 616–629, http://doi.org/10.1029/1999TC001145.

Barth, A.P., Wooden, J.L., and Coleman, D.S., 2001, SHRIMP-RG U-Pb zircon geochronology of Mesoproterozoic metamorphism and plutonism in the southwesternmost United States: The Journal of Geology, v. 109, no. 3, p. 319–327, http://doi.org/10.1086/319975.

Barth, A.P., Anderson, J.L., Jacobson, C.E., Paterson, S., and Wooden, J.L., 2008, Magmatism and tectonics in a tilted crustal section through a continental arc, eastern Transverse Ranges and southern Mojave Desert, in Duebendorfer, E.M., and Smith, E.I., eds., Field Guide to Plutons, Volcanoes, Faults, Reefs, Dinosaurs, and Possible Glaciation in Selected Areas of Arizona, California, and Nevada: Geological Society of America Field Guide 11, p. 101–117.

Barth, A.P., Walker, J.D., Wooden, J.L., Riggs, N.R., and Schweickert, R.A., 2011, Birth of the Sierra Nevada magmatic arc: Early Mesozoic plutonism and volca-

nism in the east-central Sierra Nevada of California: Geosphere, v. 7, no. 4, p. 877–897, http://doi.org/10.1130/GES00661.1.

Barth, A.P., Wooden, J.L., Jacobson, C.E., and Economos, R.C., 2013, Detrital zircon as a proxy for tracking the magmatic arc system: The California arc example: Geology, v. 41, no. 2, p. 223–226, http://doi.org/10.1130/G33619.1.

Barth, A.P., Wooden, J.L., Miller, D.M., Howard, K.A., Fox, L.K., Schermer, E.R., and Jacobson, C.E., 2017, Regional and temporal variability of melts during a Cordilleran magma pulse: Age and chemical evolution of the Jurassic arc, eastern Mojave Desert, California: Geological Society of America Bulletin, v. 129, no. 3-4, p. 429–448, http://doi.org/10.1130/B31550.1.

Beckerman, G.M., Robinson, J.P., and Anderson, J.L., 1982, The Teutonia batholith: A large intrusive complex of Jurassic and Cretaceous age in the eastern Mojave Desert, California, in Frost, E.G., and Martin, D.L., eds., Mesozoic–Cenozoic Tectonic Evolution of the Colorado River Region, California, Arizona and Nevada: San Diego, California, USA, Cordilleran Publishers, p. 205–221.

Bloomer, S.H., Stern, R.J., Fisk, E., and Geschwind, C.H., 1989, Shoshonitic volcanism in the Northern Mariana Arc 1. Mineralogic and major and trace element characteristics: Journal of Geophysical Research, v. 94, p. 4469–4496.

Brown, H.J., Stone, P., Cecil, M.R., and Fitzpatrick, J., 2018, New insights into the geology of the Lane Mountain and North Calico Mountains area, central Mojave Desert, California: Geological Society of America Abstracts with Programs, v. 50, no. 5, http://doi.org/10.1130/abs/2018RM-311369.

Burchfiel, B.C., and Davis, G.A., 1972, Structural framework and evolution of the southern part of the Cordilleran orogeny, western United States: American Journal of Science, v. 272, no. 2, p. 97–118, http://doi.org/10.2475/ajs.272.2.97.

Burchfiel, B.C., and Davis, G.A., 1975, Nature and controls of Cordilleran orogenesis, Western United States: Extensions of an earlier synthesis: American Journal of Science, v. A275, p. 363–396.

Burchfiel, B.C., and Davis, G.A., 1981, Mojave Desert and environs, in Ernst, W.G., ed., The Geotectonic Development of California, Rubey Symposium volume 1: Englewood Cliffs, New Jersey, USA, Prentice Hall, p. 217–252.

Busby-Spera, C.J., 1984, Large-volume rhyolite ash flow eruptions and submarine caldera collapse in lower Mesozoic Sierra Nevada, California: Journal of Geophysical Research, v. 89, p. 8417–8427.

Carr, M.D., Poole, F.G., Harris, A.G., and Christiansen, R.L., 1981, Western facies Paleozoic rocks in the Mojave Desert, California, in Howard, K.A., Carr, M.D., and Miller, D.M., eds., Tectonic Framework of the Mojave and Sonoran Deserts, California and Nevada: U.S. Geological Society Open-File Report 81-503, p. 15–17.

Carr, M.D., Christiansen, R.L., and Poole, F.G., 1984, Pre-Cenozoic geology of the El Paso Mountains, southwestern Great Basin, California, in Lintz, J., ed., Western Geological Excursions Volume 4: Reno, Nevada, USA, Mackay School of Mines, p. 84–93.

Carr, M.D., Harris, A.G., Poole, F.G., and Fleck, R.J., 1992, Stratigraphy and structure of Paleozoic outer continental-margin rocks in Pilot Knob Valley, north-central Mojave Desert, California: U.S. Geological Survey Bulletin, v. 2015, 33 p.

Carr, M.D., Christiansen, R.L., Poole, F.G., and Goodge, J.W., 1997, Bedrock geologic map of the El Paso Mountains in the Garlock and El Paso peaks 7-1/2′ quadrangles, Kern County, California. U.S. Geological Survey Miscellaneous Investigation Series Map 1-2389, scale 1:24,000, 1 sheet, 9 p. text.

Chapman, A.D., Saleeby, J.B., Wood, D.J., Piasecki, A., Kidder, S., Ducea, M.N., and Farley, K.A., 2012, Late Cretaceous gravitational collapse of the southern Sierra Nevada batholith, California: Geosphere, v. 8, no. 2, p. 314–341, http://doi.org/10.1130/GES00740.1.

Chapman, A.D., Ernst, W.G., Gottlieb, E., Powerman, V., and Metzger, E.P., 2015, Detrital zircon geochronology

of Neoproterozoic–Lower Cambrian passive-margin strata of the White-Inyo Range, east-central California: Implications for the Mojave-Snow Lake fault hypothesis: Geological Society of America Bulletin, v. 127, p. 926–944, http://doi.org/10.1130/B31142.1.

Christiansen, R.L., 1961, Structure, Metamorphism, and Plutonism of the El Paso Mountains, Mojave Desert, California [Ph.D. thesis]: Stanford University, Stanford, California, USA, 180 p.

Coleman, D.S., Barth, A.P., and Wooden, J.L., 2002, Early to Middle Proterozoic construction of the Mojave province, southwestern United States: Gondwana Research, v. 5, no. 1, p. 75–78, http://doi.org/10.1016/S1342-937X(05)70890-X.

Cox, B.F., and Morton, J.L., 1980, Late Permian plutonism in the El Paso Mountains, California: Geological Society of America Abstracts with Programs, v. 12, p. 103.

DeCelles, P.G., Ducea, M.N., Kapp, P., and Zandt, G., 2009, Cyclicity in Cordilleran orogenic systems: Nature Geoscience, v. 2, no. 4, p. 251–257, http://doi.org/10.1038/ngeo469.

Dibblee, T.W., 1967, Areal geology of the western Mojave Desert, California: U.S. Geological Survey Professional Paper 522, 153 p., https://doi.org/10.3133/pp522.

Dibblee, T.W., and Minch, J.A., 2008, Geologic map of the Cross Mountain and Saltdale 15 minute quadrangles, Kern County, California: Dibblee Geologic Foundation Map DF-399, scale 1:62,500.

Dickinson, W.R., 2000, Geodynamic interpretation of Paleozoic tectonic trends oriented oblique to the Mesozoic Klamath-Sierran continental margin in California, *in* Soreghan, M.J., and Gehrels, G., eds., Paleozoic and Triassic Paleogeography and Tectonics of Western Nevada and Northern California: Geological Society of America Special Paper 347, p. 209–245, http://doi.org/10.1130/0-8137-2347-7.209.

Dickinson, W.R., 2004, Evolution of the North American Cordillera: Annual Review of Earth and Planetary Sciences, v. 32, no. 1, p. 13–45, http://doi.org/10.1146/annurev.earth.32.101802.120257.

Dickinson, W.R., and Lawton, T.F., 2001, Carboniferous to Cretaceous assembly and fragmentation of Mexico: Geological Society of America Bulletin, v. 113, no. 9, p. 1142–1160, http://doi.org/10.1130/0016-7606(2001)113<1142:CTCAAF>2.0.CO;2.

Dokka, R.K., 1989, The Mojave extensional belt of southern California: Tectonics, v. 8, p. 363–390, http://doi.org/10.1029/TC008i002p00363.

Domeier, M., and Torsvik, T.H., 2014, Plate tectonics in the Paleozoic: Geoscience Frontiers, v. 5, p. 303–350, http://doi.org/10.1016/j.gsf.2014.01.002.

Drew, S.T., Ducea, M.N., and Schoenbohm, L.M., 2009, Mafic volcanism on the Puna Plateau, NW Argentina: Implications for lithospheric composition and evolution with an emphasis on lithospheric foundering: Lithosphere, v. 1, no. 5, p. 305–318, http://doi.org/10.1130/L54.1.

Ducea, M.N., 2001, The California arc: Thick granitic batholiths, eclogitic residues, lithospheric-scale thrusting, and magmatic flare-ups: GSA Today, v. 11, no. 11, p. 4–10, http://doi.org/10.1130/1052-5173(2001)011<0004:TCATGB>2.0.CO;2.

Ducea, M.N., Saleeby, J.B., and Bergantz, G., 2015a, The Architecture, Chemistry, and Evolution of Continental Magmatic Arcs: Annual Review of Earth and Planetary Sciences, v. 43, no. 1, p. 299–331, http://doi.org/10.1146/annurev-earth-060614-105049.

Ducea, M.N., Otamendi, J.E., Bergantz, G., Jianu, D., and Petrescu, L., 2015b, The origin and petrologic evolution of the Ordovician Famatinian-Puna arc, *in* DeCelles, P.G., Ducea, M.N., Carrapa, B., and Kapp, P.A., eds., Geodynamics of a Cordilleran Orogenic System: The Central Andes of Argentina and Northern Chile: Boulder, Colorado, USA, Geological Society of America, v. 212, p. 125–138, http://doi.org/10.1130/2015.1212(07).

Ducea, M.N., Bergantz, G., Crowley, J.L., and Otamendi, J.E., 2017, Ultrafast magmatic buildup and diversification to produce continental crust during subduction: Geology, v. 45, p. 235–238, http://doi.org/10.1130/G38726.1.

Dunne, G.C., and Suczek, C.A., 1991, Early Paleozoic eugeoclinal strata in the Kern Plateau pendants, southern Sierra Nevada, California, *in* Cooper, J. D., and Stevens, C. H., eds., Paleozoic Paleogeography of the Western United States, Volume Book 67, Pacific Coast Paleogeography Symposium 2: Los Angeles, California, USA, Pacific Section, Society of Economic Paleontologists and Mineralogists, p. 677–692.

Fleck, R.J., 1990, Neodymium, strontium and trace-element evidence of crustal anatexis and magma mixing in the Idaho batholith, *in* Anderson, J.L., ed., The Nature and Origin of Cordilleran Magmatism: Geological Society of America Memoir 174, p. 359–373, http://doi.org/10.1130/MEM174-p359.

Fleck, R.J., and Criss, R.E., 1985, Strontium and oxygen isotopic variations in Mesozoic and Tertiary plutons of central Idaho: Contributions to Mineralogy and Petrology, v. 90, p. 291–308.

Gehrels, G.E., Dickinson, W.R., Riley, B.C.D., Finney, S.C., and Smith, M.T., 2000, Detrital zircon geochronology of the Roberts Mountain allochthon, *in* Soreghan, M.J., and Gehrels, G.E., eds., Paleozoic and Triassic paleogeography and tectonics of western Nevada and northern California: Geological Society of America Special Paper 347, p. 19–42.

Gerber, M.E., Miller, C.F., and Wooden, J.L., 1995, Plutonism at the eastern edge of the Cordilleran Jurassic magmatic belt, Mojave Desert, California, *in* Miller, D.M., and Busby, C., eds., Jurassic Magmatism and Tectonics of the North American Cordillera, Geological Society of America Special Paper 299, p. 351–374, http://doi.org/10.1130/SPE299-p351.

Glazner, A.F., Bartley, J.M., and Walker, J.D., 1989, Magnitude and significance of Miocene crustal extension in the central Mojave Desert, California: Geology, v. 17, p. 50–53, http://doi.org/10.1130/0091-7613(1989)017<0050:MASOMC>2.3.CO;2.

Glazner, A.F., Walker, J.D., Bartley, J.M., and Fletcher, J.M., 2002, Cenozoic evolution of the Mojave block of southern California, *in* Glazner, A.F., Walker, J.D., and Bartley, J.M., eds., Geologic Evolution of the Mojave Desert and Southwestern Basin and Range: Geological Society of America Memoir 195, p. 19–41, http://doi.org/10.1130/0-8137-1195-9.19.

Gurnis, M., Hall, C.E., and Lavier, L.L., 2004, Evolving force balance during incipient subduction: Geochemistry, Geophysics, Geosystems, v. 5, no. 7, http://doi.org/10.1029/2003GC000681.

Hall, C.E., Gurnis, M., Sdrolias, M., and Lavier, L.L., 2003, Catastrophic initiation of subduction following forced convergence across fracture zones: Earth and Planetary Science Letters, v. 212, p. 15–30, http://doi.org/10.1016/S0012-821X(03)00242-5.

Kylander-Clark, A.R.C., Hacker, B.R., and Cottle, J.M., 2013, Laser-ablation split-stream ICP petrochronology: Chemical Geology, v. 345, p. 99–112, http://doi.org/10.1016/j.chemgeo.2013.02.019.

Lallemand, S., Heuret, A., and Boutelier, D., 2005, On the relationships between slab dip, back-arc stress, upper plate absolute motion, and crustal nature in subduction zones: Geochemistry, Geophysics, Geosystems, v. 6, no. 9, http://doi.org/10.1029/2005GC000917.

Lange, R.A., and Carmichael, I.S.E., 1991, A potassic volcanic front in western Mexico: The lamprophyric and related lavas of San Sabastian: Geological Society of America Bulletin, v. 103, p. 928–940, http://doi.org/10.1130/0016-7606(1991)103<0928:APVFIW>2.3.CO;2.

Leng, W., and Gurnis, M., 2011, Dynamics of subduction initiation with different evolutionary pathways: Geochemistry, Geophysics, Geosystems, v. 12, no. 12, http://doi.org/10.1029/2011GC003877.

Martin, M.W., and Walker, J.D., 1992, Extending the western North American Proterozoic and Paleozoic continental crust through the Mojave Desert: Geology, v. 20, no. 8, p. 753–756, http://doi.org/10.1130/0091-7613(1992)020<0753:ETWNAP>2.3.CO;2.

Martin, M.W., and Walker, J.D., 1995, Stratigraphy and paleogeographic significance of metamorphic rocks in the Shadow Mountains, western Mojave Desert, California: Geological Society of America Bulletin, v. 107, no. 3, p. 354–366, http://doi.org/10.1130/0016-7606(1995)107<0354:SAPSOM>2.3.CO;2.

Martin, M.W., Glazner, A.F., Walker, J.D., and Schermer, E.R., 1993, Evidence for right-lateral transfer faulting accommodating en echelon Miocene extension, Mojave Desert, California: Geology, v. 21, p. 355–358.

McDonald, E.K., Cecil, M.R., Marsaglia, K.M., Heermance, R.V., and Riggs, N.R., 2016, Stratigraphy and detrital zircon geochronology of the El Paso Mountains Permian metasedimentary sequence, southern California: A unique record of arc emergence along southwestern Laurentia: Geological Society of America Abstracts with Programs, v. 48, no. 7, https://doi.org/10.1130/abs/2016AM-282233.

Miller, E.L., and Sutter, J.F., 1982, Structural geology and ^{40}Ar-^{39}Ar geochronology of the Goldstone Lane Mountain area, Mojave Desert, California: Geological Society of America Bulletin, v. 93, no. 12, p. 1191–1207, http://doi.org/10.1130/0016-7606(1982)93<1191:SGAAGO>2.0.CO;2.

Miller, F.K., and Morton, D.M., 1980, Potassium-argon geochronology of the Transverse Ranges and southern Mojave Desert, southern California: U.S. Geological Survey Professional Paper, v. 1152, 30 p., https://doi.org/10.3133/pp1152.

Miller, J.S., and Glazner, A.F., 1995, Jurassic plutonism and crustal evolution in the central Mojave Desert, California: Contributions to Mineralogy and Petrology, v. 118, no. 4, p. 379–395, http://doi.org/10.1007/s004100050021.

Miller, J.S., Glazner, A.F., Walker, J.D., and Martin, M.W., 1995, Geochronological and isotopic evidence for Triassic–Jurassic emplacement of the eugeoclinal allocthon in the Mojave Desert region, California: Geological Society of America Bulletin, v. 107, no. 12, p. 1441–1457, http://doi.org/10.1130/0016-7606(1995)107<1441:GAIEFT>2.3.CO;2.

Miller, J.S., Glazner, A.F., Farmer, G.L., Suayah, I.B., and Keith, L.A., 2000, A Sr, Nd, and Pb isotopic study of mantle domains and crustal structure from Miocene volcanic rocks in the Mojave Desert, California: Geological Society of America Bulletin, v. 112, no. 8, p. 1264–1279, http://doi.org/10.1130/0016-7606(2000)112<1264:ASNAPI>2.0.CO;2.

Otamendi, J.E., Ducea, M.N., Tibaldi, A.M., Bergantz, G.W., de la Rosa, J.D., and Vujovich, G.I., 2009, Generation of tonalitic and dioritic magmas by coupled partial melting of gabbroic and metasedimentary rocks within the deep crust of the Famatinian magmatic arc, Argentina: Journal of Petrology, v. 50, no. 5, p. 841–873, http://doi.org/10.1093/petrology/egp022.

Paterson, S.R., and Ducea, M.N., 2015, Arc magmatic tempos: Gathering the evidence: Elements (Quebec), v. 11, no. 2, p. 91–98, http://doi.org/10.2113/gselements.11.2.91.

Paterson, S.R., Okaya, D., Memeti, V., Economos, R., and Miller, R.B., 2011, Magma addition and flux calculations of incrementally constructed magma chambers in continental margin arcs: Combined field, geochronologic, and thermal modeling studies: Geosphere, v. 7, no. 6, p. 1439–1468, http://doi.org/10.1130/GES00696.1.

Poole, F.G., and Sandberg, C.A., 1977, Mississippian paleogeography and tectonics of the western United States, *in* Stewart, J.H., Stevens, C.H., and Fritsche, A.E., eds., Paleozoic Paleogeography of the Western United States Los Angeles, California, Pacific Section: Society of Economic Paleontologists and Mineralogists, Pacific Coast Paleogeography Symposium 1, p. 67–85.

Premo, W.R., Morton, D.M., Wooden, J.L., and Fanning, C.M., 2014, U-Pb zircon geochronology of plutonism in the northern Peninsular Ranges batholith, southern California: Implications for the Late Cretaceous tectonic evolution of southern California, *in* Morton, D.M., and Miller, F.K., eds., Peninsular Ranges Batholith, Baja California and Southern California: Geological Society of America Memoir 211, p. 145–180, http://doi.org/10.1130/2014.1211(04).

Rains, J.L., Marsaglia, K.M., and Dunne, G.C., 2012, Stratigraphic record of subduction initiation in the Permian

metasedimentary succession of the El Paso Mountains, California: Lithosphere, v. 4, no. 6, p. 533–552, http://doi.org/10.1130/L165.1.

Riggs, N.R., Barth, A.P., Gonzalez-Leon, C.M., Walker, J.D., and Wooden, J.L., 2009, Provenance of Upper Triassic strata in southwestern North America as suggested by isotopic analysis and chemistry of zircon crystals: Geological Society of America Abstracts with Programs, v. 41, no. 7, p. 540.

Riggs, N.R., Reynolds, S.J., Lindner, P.J., Howell, E.R., Barth, A.P., Parker, W.G., and Walker, J.D., 2013, The Early Mesozoic Cordilleran arc and Late Triassic paleotopography: The detrital record in Upper Triassic sedimentary successions on and off the Colorado Plateau: Geosphere, v. 9, no. 3, p. 602–613, http://doi.org/10.1130/GES00860.1.

Riggs, N.R., Gonzalez-Leon, C.M., Cecil, M.R., Marsaglia, K.M., and Navas-Parejo, P., 2014, Age of the Permian Monos Formation, northern Sonora, Mexico, and implications for initiation of the Cordilleran magmatic arc: Geological Society of America Abstracts with Programs, v. 46, no. 6, p. 377.

Riggs, N.R., Oberling, Z.A., Howell, E.R., Parker, W.G., Barth, A.P., Cecil, M.R., and Martz, J.W., 2016a, Sources of volcanic detritus in the basal Chinle Formation, southwestern Laurentia, and implications for the Early Mesozoic magmatic arc: Geosphere, v. 12, no. 2, p. 439–463, http://doi.org/10.1130/GES01238.1.

Riggs, N.R., Barth, A.P., Walker, J.D., Lindner, P., Gonzalez-Leon, C., Cecil, M. Robinson, and Marsaglia, K.M., 2016b, Implications of Permian magmatism in southwest Laurentia for tectonic reconstructions: Geological Society of America Abstracts with Programs, v. 48, no. 7, http://doi.org/10.1130/abs/2016AM-279985.

Rioux, M., B. R. Hacker, J. Mattinson, P. Kelemen, J. Blusztajn, and G. Gehrels, 2007, Magmatic development of an intra-oceanic arc: High-precision U-Pb zircon and whole-rock isotopic analyses from the accreted Talkeetna arc, south-central Alaska: Geological Society of America Bulletin, v. 119, p. 1168–1184.

Saleeby, J., 2011, Geochemical mapping of the Kings-Kaweah ophiolite belt, California: Evidence for progressive mélange formation in a large offset transform-subduction initiation environment, *in* Wakabayashi, J., and Dilek, E., eds., Mélanges: Processes of Formation and Societal Significance: Geological Society of America Special Paper 480, p. 31–73, http://doi.org/10.1130/2011.2480(02).

Saleeby, J., and Busby-Spera, C.J., 1992, Early Mesozoic tectonic evolution of the western U.S. Cordillera, *in* Burchfiel, B.C., Lipman, P.W., and Zoback, M.L., eds., The Cordilleran Orogen: Conterminous U.S.: Boulder, Colorado, USA, Geological Society of America, The Geology of North America, v. G-3, p. 107–168.

Saleeby, J., and Dunne, G., 2015, Temporal and tectonic relations of early Mesozoic arc magmatism, southern Sierra Nevada, California, *in* Anderson, T.H., Didenko, A.N., Johnson, C.L., Khanchuk, A.I., and MacDonald Jr., J.H., eds., Late Jurassic Margin of Laurasia: A Record of Faulting Accommodating Plate Rotation:

Geological Society of America Special Paper 513, p. 223–268, http://doi.org/10.1130/2015.2513(05).

Saleeby, J., and Sharp, W., 1980, Chronology of the structural and petrologic development of the southwest Sierra Nevada foothills, California: Summary: Geological Society of America Bulletin, v. 91, no. 6, p. 317–320, http://doi.org/10.1130/0016-7606(1980)91<317:COTSAP>2.0.CO;2.

Schermer, E.R., and Busby, C., 1994, Jurassic magmatism in the central Mojave Desert: Implications for arc paleogeography and preservation of continental volcanic sequences: Geological Society of America Bulletin, v. 106, no. 6, p. 767–790, http://doi.org/10.1130/0016-7606(1994)106<0767:JMITCM>2.3.CO;2.

Smith, M., and Gehrels, G., 1994, Detrital zircon geochronology and the provenance of the Harmony and Valmy Formations, Roberts Mountain Allochthon, Nevada: Geological Society of America Bulletin, v. 106, no. 7, p. 968–979, http://doi.org/10.1130/0016-7606(1994)106<0968:DZGATP>2.3.CO;2.

Stern, R.J., 2004, Subduction initiation: Spontaneous and induced: Earth and Planetary Science Letters, v. 226, p. 275–292, http://doi.org/10.1016/S0012-821X(04)00498-4.

Stern, R.J., Bloomer, S.H., Lin, P., Ito, E., and Morris, J., 1988, Shoshonitic magmas in nascent arcs: New evidence from submarine volcanoes in the northern Marianas: Geology, v. 16, p. 426–430, http://doi.org/10.1130/0091-7613(1988)016<0426:SMINAN>2.3.CO;2.

Stevens, C.H., and Stone, P., 1988, Early Permian thrust faults in east-central California: Geological Society of America Bulletin, v. 100, no. 4, p. 552–562, http://doi.org/10.1130/0016-7606(1988)100<0552:EPTFIE>2.3.CO;2.

Stevens, C.H., and Stone, P., 2005, Structure and regional significance of the Late Permian(?) Sierra Nevada-Death Valley thrust system, east-central California: Earth-Science Reviews, v. 73, no. 1-4, p. 103–113, http://doi.org/10.1016/j.earscirev.2005.04.006.

Stevens, C.H., Stone, P., and Miller, J.S., 2005, A new reconstruction of the Paleozoic continental margin of southwestern North America: Implications for the nature and timing of continental truncation and the possible role of the Mojave-Sonora megashear, *in* Anderson, T.H., Nourse, J.A., McKee, J.W., and Steiner, M.B., eds., The Mojave-Sonora Megashear Hypothesis: Development, Assessment, and Alternatives: Geological Society of America Special Paper 393, p. 597–618, http://doi.org/10.1130/0-8137-2393-0.597.

Stewart, J.H., and Poole, F.G., 1975, Extension of Cordilleran miogeosynclinal belt to San Andreas Fault, southern California: Geological Society of America Bulletin, v. 86, no. 2, p. 205–212, http://doi.org/10.1130/0016-7606(1975)86<205:EOTCMB>2.0.CO;2.

Stone, P., and Stevens, C.H., 1988, Pennsylvanian and Early Permian paleogeography of east-central California: Implications for the shape of the continental margin and the timing of continental truncation: Geology, v. 16, no. 4, p. 330–333, http://doi.org/10.1130/0091-7613(1988)016<0330:PAEPPO>2.3.CO;2.

Sun, S., and McDonough, W.F., 1989, Chemical and isotopic systematics of ocean basalts: Implications for mantle composition and processes, *in* Saunders, A.D., and Norry, M.J., eds., Magmatism in the Oceanic Basins: Geological Society of London Special Publications 42, p. 313–345, http://doi.org/10.1144/GSL.SP.1989.042.01.19.

Walker, B.A., Bergantz, G., Otamendi, J.E., Ducea, M.N., and Cristofolini, E.A., 2015, A MASH zone revealed: The mafic complex of the Sierra Valle Fértil: Journal of Petrology, v. 56, p. 1863–1896, http://doi.org/10.1093/petrology/egv057.

Walker, J.D., 1988, Permian and Triassic rocks of the Mojave Desert and their implications for the timing and mechanisms of continental truncation: Tectonics, v. 7, no. 3, p. 685–709, http://doi.org/10.1029/TC007i003p00685.

Walker, J.D., Bartley, J.M., and Glazner, A.F., 1990, Large-magnitude Miocene extension in the central Mojave Desert: Implications for Paleozoic to Tertiary paleogeography and tectonics: Journal of Geophysical Research, v. 95, p. 557–569, http://doi.org/10.1029/JB095iB01p00557.

Wetmore, P., and Ducea, M.N., 2011, Geochemical evidence of a near-surface history for source rocks of the central Coast Mountains batholith, British Columbia: International Geology Review, v. 53, p. 230–260, http://doi.org/10.1080/00206810903028219.

White, W.M., 2010, Oceanic island basalts and mantle plumes: The geochemical perspective: Annual Review of Earth and Planetary Sciences, v. 38, p. 133–160, http://doi.org/10.1146/annurev-earth-040809-152450.

Wooden, J.L., and Miller, D.M., 1990, Chronological and isotopic framework for early Proterozoic crustal evolution in the eastern Mojave Desert region, SE California: Journal of Geophysical Research-Solid Earth and Planets, v. 95, p. 20133–20146, http://doi.org/10.1029/JB095iB12p20133.

Wooden, J.L., Barth, A.P., and Mueller, P.A., 2013, Crustal growth and tectonic evolution of the Mojave crustal province: Insights from hafnium isotope systematics in zircons: Lithosphere, v. 5, no. 1, p. 17–28, http://doi.org/10.1130/L218.1.

Workman, R.K., and Hart, S.R., 2005, Major and trace element composition of the MORB mantle (DMM): Earth and Planetary Science Letters, v. 231, p. 53–72, http://doi.org/10.1016/j.epsl.2004.12.005.

Zuo, X., Chan, L.S., and Gao, J.F., 2017, Compression-extension transition of continental crust in a subduction zone: A parametric numerical modeling study with implications on Mesozoic-Cenozoic tectonic evolution of the Cathaysia Block: PLoS One, v. 12, http://doi.org/10.1371/journal.pone.0171536.